Iron oxide nanoparticles – In vivo/in vitro biomedical applications and in silico studies

Miroslava Nedyalkova, Borjana Donkova, Julia Romanova, George Tzvetkov, Sergio Madurga, Vasil Simeonov

PII: S0001-8686(17)30083-0
DOI: doi: 10.1016/j.cis.2017.05.003
Reference: CIS 1754

To appear in: *Advances in Colloid and Interface Science*

Received date: 1 February 2017
Revised date: 28 April 2017
Accepted date: 2 May 2017

Please cite this article as: Miroslava Nedyalkova, Borjana Donkova, Julia Romanova, George Tzvetkov, Sergio Madurga, Vasil Simeonov , Iron oxide nanoparticles – In vivo/ in vitro biomedical applications and in silico studies, *Advances in Colloid and Interface Science* (2016), doi: 10.1016/j.cis.2017.05.003

Iron Oxide Nanoparticles –*In vivo*/*In vitro* Biomedical Applications *and In silico* studies

Miroslava Nedyalkova[a]*, Borjana Donkova[a], Julia Romanova[a], George Tzvetkov[a], Sergio Madurga[b], Vasil Simeonov[a]

[a] Faculty of Chemistry and Pharmacy, University of Sofia "St. Kl. Okhridski". J. Bourchier Blvd. 1, 1164 Sofia, Bulgaria

[b] Materials Science and Physical Chemistry Department & Research Institute of Theoretical and Computational Chemistry (IQTCUB) of Barcelona University (UB), C/ Martí i Franquès, 1. 08028 Barcelona, Catalonia, Spain

*Corresponding author at: Faculty of Chemistry and Pharmacy, University of Sofia "St. Kl. Okhridski". J. Bourchier Blvd. 1, 1164 Sofia, Bulgaria

Tel.: +359 885 76 33 98

E-mail: mici345@yahoo.com

Abstract: The review presents a broad overview of the biomedical applications of surface functionalized iron oxide nanoparticles (IONPs) as magnetic resonance imaging (MRI) agents for sensitive and precise diagnosis tool and synergistic combination with other imaging modalities. Then, the recent progress in therapeutic applications, such as hyperthermia is discussed and the available toxicity data of magnetic nanoparticles concerning *in vitro* and *in vivo* biomedical applications are addressed. This review also presents the available computer models using molecular dynamics (MD), Monte Carlo (MC) and density functional theory (DFT), as a basis for a complete understanding of the behaviour and morphology of functionalized IONPs, for improving NPs surface design and expanding the potential applications in nanomedicine.

Keywords: magnetic iron oxide nanoparticles; computational modelling; biomedical application; imaging; toxicity

Content:

1. Introduction

Iron oxide based magnetic nanoparticles (IONPs) have received remarkable attention in a wide range of applications because of their unique physicochemical properties inherent to the nanoscale. Small size, high surface area, quantum confinement, and novel magnetic and optical effects open up new fields for application of iron oxides. For instance, conventional magnetic materials (ferromagnetic iron oxides) lose their permanent magnetization if they are studied or used as nanoparticles [1, 2]. Parallel to the practical uses of magnetic IONPs in electronics and catalysis, they are widely considered since decades for magnetic hyperthermia goals (local heat source in the case of tumour therapy) [3] and as contrast agents for magnetic resonance imaging (MRI) [4, 5, 6]. Since then, the switchable magnetic properties of IONPs makes them attractive for a rapidly expanding number of bioapplications: labelling and sorting of cells, cell transfection, enhance diagnostic imaging output like in magnetic resonance imaging (MRI), positron emission tomography (PET), tissue-specific drug/gene delivery systems, for magnetic hyperthermia treatment or as multifunctional nanoplatforms for magnetic theranostic by a combination of two or more of the corresponding applications [7-10, 2].

The IONPs show ability for the biomedical application; they need to possess suitable core size and monodispersity, acceptable hydrodynamic diameter, high saturation magnetisation (M_s), high stability in biological fluid media, to be bio-compatible and degradable with reduced toxicity over a large time scale, capable of clearance from the body post imaging. The used nanosystems consist of iron oxide single-core or multi-cores and shell/s ensuring the colloidal stability in the biological environment, limiting the non-specific adsorption of biomolecules and fulfilling the roles of anchors, spacers and various functionalities. The single-core nanoparticles contain single-domain nanocrystal per particle, while the multi-core nanoparticles consist of superparamagnetic particles (~10 nm) which form moderate ferrimagnetic clusters (from 20 to 80 nm) [11].

The magnetic behaviour of IONPs is crucial for their effectiveness in biomedical applications, partially based on their superparamagnetic properties. Therefore, IONPs often are labelled as SPIONs (superparamagnetic iron oxide nanoparticles). Superparamagnetism is a property occurring principally in nanoparticles which are single-domain and can be attributed to their size [1, 2]. The dependence of magnetic properties of SPIONs on the specific composition, structure, size, size distribution, shape and thickness of surface coating are the object of extensive studies, part of which are summarised in [12-16]. The rheological behaviour of the ferrofluids

containing IONPs also is a subject of investigation, e.g. [17, 18], since the knowledge about changes under an external magnetic field to ensure safe and efficient treatment of living organisms is essential.

The procedures for synthesis/surface coating/encapsulation, their effect on the physicochemical properties, and potential field of biomedical applications of SPIONs are reviewed throughout the years [16, 19-29]. A very detailed analysis of the advantages and disadvantages of different synthesis methods is given in [27], while in reviews [16, 29] the focus is on the classification of the proven synthesis routes based on their capacity to produce either single-core or multi-core nanoparticles. The special attention is paid to the fact that the choice must obey to their specific biomedical application [29] as it is also presented in Ref. [11] because not only the magnetic properties of single- and multi-core NPs are different [11, 30], but also the rheological behaviour of the corresponding ferrofluids [17].

The main synthesis routes for the preparation of SPIONs are well established during the last two decades, and some of them like co-precipitation, mild oxidative hydrolysis and thermal decomposition are readily available for producing IONPs in semi-industrial quantities. Initially, variations in the procedures were dealing not with the core but mainly with the stages of stabilisation, as well as in the surface modification so that the final product to be biocompatible and suitable for further coupling with different features like fluorescent dyes, drugs or specific bioactive molecules. In the last decade, the studies are directly related to the final specific application of SPIONs and cover mainly: i) tuning of the magnetic properties by changing the shape, by controlling size and size distribution, by using multi-core IONPs or assembling; ii) obtaining multimodal hybrid structures for theranostic applications by surface functionalization with universal ligands iii) producing safety nanoplatforms with sufficient colloidal stability in biological media and long circulation time [31-39].

Despite the vast amount of papers and the evidences for the potential applicability of SPIONs in nanomedicine, it has to be taken into account that a limited part of the reported synthesis procedures is in resonance with the nano-safety regulatory framework, and respectively, a minor part of these innovative nanoplatforms could find real biomedical implementation [40-42]. Moreover, even some of the designed for clinical application and tested MR contrast agents did not receive regulatory approval (Clariscan®/VSOP C184). Others (Endorem®, Lumirem®/ GastroMARK®) received approval, however, they were taken off the market while some of the approved (Resovist®, Ferumoxytol) were currently available in quite few countries [43, 44].

The presented Review is widely focused on the biomedical application of iron oxide nanoparticles, considered from *in vitro, in vivo* and *in silico* aspects. The Review is organized as

follows: in the first part a brief overview of the development of magnetic iron oxide nanoparticles as MR imaging agents and their synergistic integration with other imaging modalities is given, the second part covers recent progress in the usage of SPIONs for *in vitro* and *in vivo* cancer theranostic applications; then the focus is on currently available *in vitro* and *in vivo* toxicity data. In the final part of the review, we provide an overview of the current state of the field in theoretical studies of iron oxide nanoparticles. The novelty of our vision comes from assembling broad combinations of different approaches to the subject pointed to the potential of the iron oxide nanoparticles to become a useful platform material for theranostics and personalised medicine.

2. Biomedical applications of SPIONs

2.1. Magnetic Resonance Imaging

The progressive development of new imaging modality became conceivable due to the recent progress in nanotechnology, molecular and cell biology, and imaging technologies. Diversity in types of imaging techniques has inherent advantages and disadvantages. While molecular imaging applies to various techniques such as positron emission tomography (PET), computed tomography (CT), or ultrasound, of particular interest is the magnetic resonance imaging (MRI) that provides the best spatial resolution and it is noninvasive or at least minimally invasive [19, 21].

MRI is with excellent (submillimeter) spatial resolution, and it also avoids the radiation exposure, like in PET and CT. Additionally, soft tissue contrast is outstanding, and MRI readily yields anatomical information [45]. Conventional MRI has not been applied to its full potential for the diagnosis of cancer in the general case, because of incorrect results concerning its quite low sensitivity (false-positive rate of 10% for breast cancer). By nuclear magnetic resonance and optical imaging technologies, the ability to fight with cancer could vastly enhance, and these methods still represent the mainstay of clinical imaging.

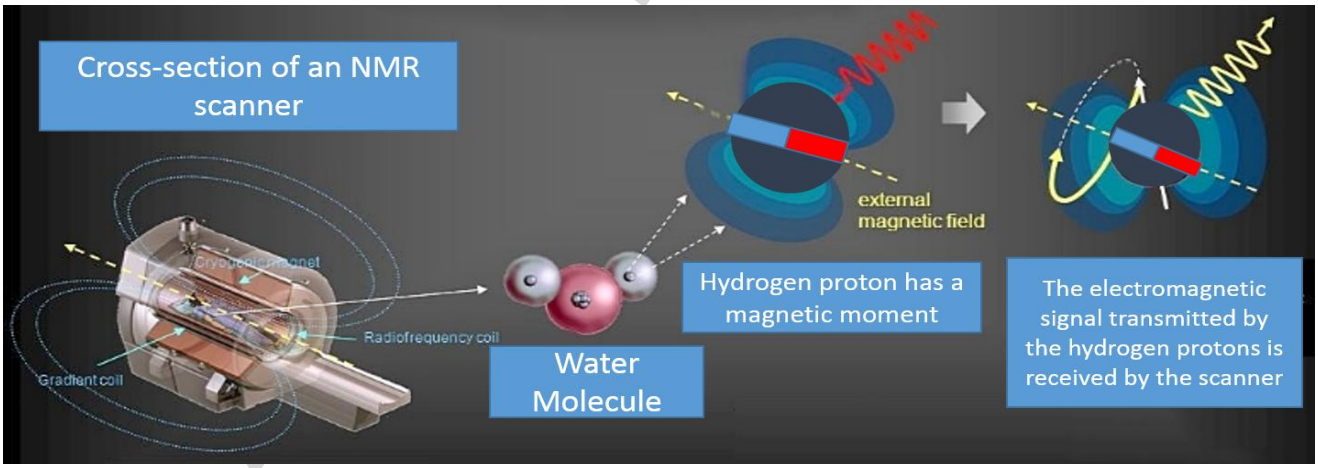

Fig. 1. Basic MRI principle: conventional MRI is based on the radiofrequency signal that is transmitted from the atomic nucleus of hydrogen atoms placed in a magnetic field and after they have been excited by a radiofrequency electromagnetic pulse ([Yves De Deene - Hyperpolarized MRI - http://slideplayer.com/slide/5049588/] and authors view).

MRI for a biomedical imaging technique used to image soft tissues of the human body in very thin slices in two-dimensional as well as three-dimensional spaces (Fig. 1). The water present in our

body plays a major role in obtaining MRI images [46]. The hydrogen nucleus in water tends to align them in a direction parallel to the applied external magnetic field. Then a radiofrequency (RF) signal is applied to change the direction of alignment of protons in the hydrogen nucleus, where the frequency of the RF signal must be in resonance with the frequency of the hydrogen nucleus. As the directions of the protons are changed after applying the RF signal, the protons tend to re-align with the applied magnetic field. So while returning to its original position, these protons release energy as an RF signal that can be detected by detectors in MRI machine. The re-alignment speed of protons varies for various tissues in our body, which is helpful in imaging such tissues precisely and the time taken for this re-alignment is called the relaxation time. Relaxation processes are two types: longitudinal relaxation (also called spin−lattice relaxation) and transverse relaxation (also called spin−spin relaxation).

The T_1 relaxation time is characterised by the time required for longitudinal magnetisation to recuperate from zero to a value of 63% of the original state. The transverse magnetisation of the protons decays as the nuclear spins is dephased, which is the transverse relaxation. The time for the transverse magnetisation and drop from the maximum to a value of 37% of its excited state value is the T_2 relaxation time. The relaxivities (r_1 and r_2), that change with the applied magnetic field in longitudinal and transverse directions, are the inverse of the relaxation times at the respective directions (i.e., $r_1 = 1/T_1$; $r_2 = 1/T_2$), where the ratio of relaxivities is significant in deciding the fate of the nanoparticles to be used either as a positive or a negative contrast. Both T_1 and T_2 relaxations are dependent on the saturation magnetisation of nanoparticles and their magnetic interactions with the protons of surrounding water molecules.

The sensitivity of MRI can be significantly improved by the agents that enhance the contrast of the region of interest from the background. Numerous parameters like size of the iron oxide crystals, type of the coating, and hydrodynamic size of the coated NPs, polydispersity, and surface charge of SPIONs as MRI contrast agents accomplish their productivity and efficiency. The colloidal stability depends in general, on these characteristics and has a significant impact on the: cellular uptake, protein adsorption and interactions with biological membranes, and biokinetic parameters such as biodistribution, biodegradation, metabolism, and elimination (see Fig. 2). Numerous examples are summarised in the reviews of Laurent, Mahmoudi, *et al.* [47, 48].

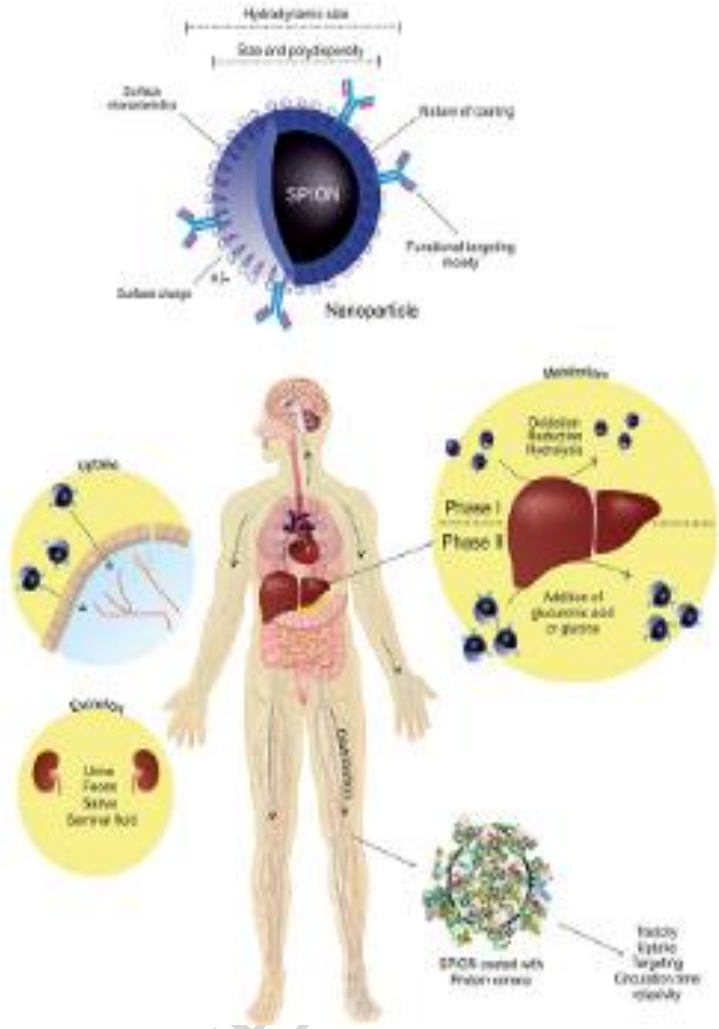

Fig. 2. The different physiochemical properties of SPIONs affect their biokinetics and fate *in vivo*. These changes can be observed in uptake, distribution, metabolism, and excretion of SPIONs from the body. Protein corona is yet another factor that is influenced by various physiochemical features of NPs and can, in turn, affect the targeting capabilities of SPIONs in imaging applications. Not only can protein corona alter the toxicity, uptake, targeting, and circulation time of SPIONs, but it can also affect the relaxivity of SPIONs as MRI contrast agents. - Reproduced from [48] with permission from the Wiley. Copyright 2015.

MRI contrast agents can be divided into two groups, i.e. positive contrast agents (or T_1-weighted contrast agents) and negative contrast agents (or T_2-weighted contrast agents). The positive contrast agents shorten the longitudinal relaxation times (T_1) of protons, resulting in a brighter image in T_1-weighted MRI and produce an increase in the NMR signal intensity. The negative contrast agents shorten both the transverse relaxation times (T_2) of protons and free induction decay time (T_2^*) leading

to the darker image in T_2- and T_2^*-weighted MRI and produce a decrease. The contrast agent does not produce a signal itself, but it marks the proton relaxation rate. Thus, the contrast between healthy and diseased tissues can be attained by varying number of protons and T_1 and T_2 relaxation times, similar to NMR. The ratio between transverse and longitudinal relaxivity (r_2/r_1) is an important parameter to estimate the efficiency of T_1 or T_2 contrast agents. The high r_2/r_1 ratio (>8) results in T_2-dominated contrast and the lower ratio (<5) leads to T_1-dominated contrast [49].

The T_1-contrast agents, approved for clinical use are prevailingly paramagnetic complexes, such as Gd^{3+} based chelates. They have low relaxivity r_2/r_1 ratio (commonly in the range of 1-2). On the contrary, the negative contrast agents are predominantly supermagnetic IONPs with a high r_2/r_1 ratio (> 5, commonly at least 10). This high relaxivity ratio limits in most cases the use of SPIONs in T_1-weighted MRI although a significant reducing of T_1 is observed, often higher as compared to the paramagnetic chelates.

However, each of clinical approved contrast agents has some disadvantages. The Gd-based chelates suffer for poor physiological stability, short life span, poor cellular uptake, nonspecificity to target and may cause induction of nephrogenic systemic fibrosis [50]. The overviews of the risks, related to the Gd-based contrast agents have been made in Refs. [51, 51]. On the other hand, although SPIONs are traditionally considered as much more efficient in MR relaxation than paramagnetic agents, their significant obstacles are magnetic susceptibility artefacts and negative contrast effects (i.e., dark MR images). Also, some of the approved for clinical use formulations had been withdrawn from the market due to the economic or safety concerns [43]. In just published literature update of clinical researchers of SPIONs for MRI [44] the opportunities and challenges for the clinical development of SPIO agents are pointed out. So, the development of novel, more efficient and safety formulations remains a challenge for the scientific community, in particular for the chemists and with the main impact of the chemical community like a driving force to move the field forward [53]. The IONPs are preferable object in research because of 1) their excellent biocompatibility; 2) the possibility of tunning their magnetic properties, respectively ratio r_2/r_1, by changing the composition, size or shape; 3) the possibility for surface modification, with different features like bioactive, therapeutic and signaling molecules, thus tailoring their application not only in imaging. Some examples of the achieved results and applicability of IONPs for MRI imaging are given, and some of the available recent published data are summarised in Table 1 in the supplement information.

2.1.1 T_1 contrast agent

For precise, high-resolution imaging, the T_1 contrast agent is more desirable than T_2. Although the SPIONs are conventionally considered as negative contrast agents, by reducing the size and preventing aggregation using proper coatings, a low magnetisation, respectively low r2 values and r2/r1 ratios could be achieved, so the SPIONs can also surve as positive contrast agents.

As explained already in the Introduction part the size greatly distresses the magnetic properties of the nanoparticles. The magnetic spins of the nanoparticle surface are disordered owing to the unique state of the surface atoms, which is called the spin-canting effect [54, 55]. The canted spins can be enhanced by reducing the size of nanoparticles because of the intensification of the spin-canting layer portion in the nanoparticles, and this is the basis for the T_1 contrast effect.

The inter-relationship between the size, magnetisation and spin-canted surface layer can be express by Eq. (1)

$$m_s = M_s[(r\text{-}d/r)]^3 \qquad (1),$$

where m_s is saturation magnetisation of the size-reduced nanoparticle, M_s is saturation magnetisation of the bulk materials, r is the size of nanoparticle and d is the thickness of the disordered surface layer. Kim *et al.* [56] estimated that about 93.6% of the surface spins in 3-nm sized iron oxide nanoparticles were canted as compared to 38.6% of surface spins in 12-nm sized nanoparticles. As a result of the increased canting effects in 3 nm sized iron oxide nanoparticles, the magnetisation values decreased correspondingly. As the size of the particle decreases to < 3 nm, the magnetic spins are canted, thus, the overall magnetic behaviour is nearly paramagnetic.

The other important factor for the T_1 performance of coated SPIONs is their dispersion state in colloidal solution. A small fraction of aggregation should drastically shorten the transverse relaxation time of the SPIONs because of increased dipolar magnetic interactions between them and thus compromise the T_1 performance [37, 57].

It has been shown that small-sized iron oxide-based nanoparticles with an overall diameter below 50 nm and core size of approximately up to 5 nm possess a potential to be utilised as high-resolution T_1-blood pool agents [58, 59, 61]. *In vivo* studies confirm their potential for MRI angiography. The most importance, in this case, is to extend their circulation time by ensuring full dispersion and long-term colloidal stability. The visualisation of blood vessels and vascular organs are demonstrated in Refs. [64-68].]

In the recent review by Shen *et al.* [65] the authors summarised liquid-based synthesis methods for production of magnetic iron oxide nanoparticles (MIONs) and extremely small magnetic iron oxide nanoparticles (ES-MIONs), and listed their applicability as T_1 and T_2 MRI contrast agents. The focus of the review is on the results for ES-MIONs (< 5 nm) and they are considered as the possible future generation of T_1 MRI contrast agents, which avoid the both disadvantages of Cd-chelate-based T_1- and MIONs-based (>10 nm) T_2- contrast agents.

The nanoparticles with bigger core size, however, could also act as an excellent positive contrast agent if good colloidal stability is observed, as it has been shown by Borase *et al.*[66]. The team prepared monodisperse galactose-coated SPIONs (core size 8.3 nm) with further potential for targeting, applying a novel combination of a polymer "grafting-from" approach with glycosylation by click chemistry. The as-prepared probes exhibit a very high r_1 value of 16 mM^{-1} s^{-1} and although the r_2/r_1 ratio is 3.9 the T_1-weighting potential remains because grafting-from/click-functionalization strategy provides a robust and adaptable chemistry that ensures optimal colloidal properties.

The effect of coatings on the T_1 performance of bigger SPIONs is also demonstrated in the recent work of Wan *et al.* [37]. The 8.5 nm SPIONs with narrow size distribution are synthesised by polyol process and further stabilised with sodium tripolyphosphate (STPP). For comparison, the same SPIONs are coated with sodium citrate. The polyanionic nature of STPP and its strong coordination capability to iron oxide warrant the SPIONs longterm colloidal stability (for years), while citrate-capped SPIONs started to precipitate after several months. In addition, although the r_1 relaxivity of STPP- and citrate-capped SPIONs are almost the same under a magnetic field of 1.41 T (18.88 and 18.69 $mM^{-1}s^{-1}$), the r_2/r_1 ratio is different being of 3.87 and 6.55, respectively. Thus the minimised aggregation of the STPP-capped SPIONs successfully suppresses the T_2 contrast effect, leading to optimised relaxometry properties for T_1-weighted MRI, which is confirmed by *in vivo* tests with a mouse model.

The composition of the nanoparticles used is another important parameter for achieving the T_1 contrast effect. Ling *et al.* [67] successfully visualised very small tumours (<3 nm) in mice via simultaneous pH-responsive T_1 MR and fluorescence imaging, thus demonstrating the possibility for early stage diagnosis of tumours without using any targeting agents. These unique tumour pH-sensitive magnetic nanogrenades (PMNs) with a diameter of 70 nm are composed of self-assembled ES-MIONs (~ 3 nm) and pH-responsive polymeric ligands. For comparison, the pH-insensitive nanoparticle assemblies are also produced and studied. At neutral conditions, PMNs show high r_2 relaxivity because of the clustering of nanoparticles, preventing an effective T_1 contrast effect. The decrease in pH from

7.4 to 5.5 leads to slight increasing of r_1 and significant decreasing of r_2/r_1 ratio only for PMNs, thus demonstrating their applicability for T_1 MR imaging of acidic tumour regions. Moreover, it is established that accumulation of PMNs in tumours is >2-fold higher than that of pH-insensitive nanoparticle assemblies, and the team successfully perform *in vivo* pH-dependant photodynamic therapy to selectively kill cancer cells.

In just available work of Zhang *et al.* [68] the correlations between the composition, size and MR T_1 signal enhancement is investigated by comparison of $MnFe_2O_4$ nanoparticles with different sizes (2, 3, 3.9, 6) with Fe_2O_3 (3 nm), MnO (7 nm) and Gd-based contrast agents. Moreover, the authors report a general dynamic simultaneous thermal decomposition strategy to couple the multicomponent chemical doping process with the nucleation process, which allows controllable synthesis of monodisperse ultrasmall metal ferrites nanoparticles (< 4 nm) for highly sensitive and multifunctional T_1 MR contrast agent. The procedure is suitable for large scale production of different kinds of metal ferrites nanoparticle MFe_2O_4 (M=Mn, Co, Ni, etc.). To achieve close decomposition temperature of Fe-precursor and M-oleate precursors, the authors prepared a new type of Fe-precursor with improved thermal stability, namely Fe-eruciate. Further hydrophilization with phosphorylated mPEG do not affect the particle size. The obtained by this procedure ultrasmall $MnFe_2O_4$ nanoparticles exhibit very high r_1 value, and the highest one of 8.43 $mM^{-1}s^{-1}$ is the highest measured among the ferrite nanoparticles with similar size reported so far, while the r_2/r_1 ratio is the smallest one. In contrast, the 6 nm $MnFe_2O_4$ cannot be used for T_1 imaging because of the high r_2/r_1 ratio of 46.1. In comparison with 7 nm, MnO and 3 nm Fe_2O_3 the as-synthesised ultrasmall $MnFe_2O_4$ nanoparticles possess better MR relaxation properties for positive contrast effect. *In vivo,* MRI imaging of blood pools and liver showed their better properties than Gd-based contrast agents and verified that the ultrasmall $MnFe_2O_4$ nanoparticles could be used as ultra-sensitive and multifunctional T_1 MR contrast agents for high-resolution MR imaging. The pharmacokinetic, biodistribution and excretion of the 3 nm UMFNPs indicates the safe of the UMFNPs for possible clinical trials.

As was shown above the small-sized iron oxide-based nanoparticles can be effective T_1 contrast agents. In the *in vivo* T_1-weighted magnetic resonance imaging, they showed longer circulation time than the clinically used Gd-based contrast agent, enabling high-resolution imaging. Also, comparative studies on the toxic effects and tissue damage induced by three T_1 MRI contrast agents – clinically used Gd-based contrast agent, ES-MIONs (3 nm) and MnO-NPs (15 nm) demonstrate that extremely small iron oxide nanoparticles exhibit better safety profile and more desired properties than the others [69]. The low toxicity, high r_1 relaxivity, long blood half-life, low synthetic cost and possibility for further

functionalization enable SPIONs to be competent T_1 for MRI contrast agents for various for clinical applications including diagnosis of the myocardial infarction, renal failure, atherosclerotic plaque, thrombosis, and angiogenesis of tumour cells.

2.1.2. T_2/T_2* MRI contrast agents

Even though iron oxide nanoparticles marked both the longitudinal and transverse relaxation processes, their effect on T_2 relaxation is much greater than on T_1 relaxation because their strong magnetic fields cause a rapid dephasing of the nuclei, resulting in apparent signal attenuation. The high r_2/r_1 ratio considered SPIONs as typical T_2 contrast agents. Based on their biocompatibility and powerful effects on T_2 relaxation, some formulation of developed SPIONs have been clinically approved as MRI contrast agents and suggested as a platform for synthesising materials that unify targeting, tracking, and hyperthermia treatment capability. To improve the performance of iron oxide nanoparticles the magnetic properties have been tunned by the modulation of size, shape and composition or by clustering.

The dependency of the r_2 relaxivity on the nanoparticles size is evaluated and described in details with different approaches. When the size of nanoparticles increases, three different regimes of r_2 values exist, based on theoretical studies of the effect of size on relaxivity, which are explained in the reviews of Lee *et al.* [70] and Zanganeh *et al.* [71] - motional average regime (MAR), static dephasing regime (SDR), and echo limiting regime (ELR). Size in the MAR, SDR and ELR have been predicted by the quantum mechanical outer sphere theory [72-74]. In the MAR mode [75. 76], the relaxivity *r*2 is given by Eq. (2) [81], where all of the nanoparticles were approximated and simulated as a model of spheres:

$$1/T_2 = (256\pi^2\gamma^2/405)V^*M_s^2\alpha^2 / D(1 + L/\alpha) \quad (2)$$

In the Eq. (2) γ is the proton gyromagnetic ratio, V^*, M_s, and α are the volume fraction of the iron oxide core, saturation magnetization, and the radius of iron oxide core, respectively, D is the diffusivity of water molecules, and L is the thickness of an impermeable surface coating.

For example, for spherical and quasispherical SPIONs with different coatings, the increasing of size in the range of 3 to 16 nm leads to increasing of r2 relaxivity from 2-fold up to approximately 20-fold [39, 78, 79]. The same is shown by Mohapatra *et al*. [80] for citrate coated octahedral USPIO with average diameter of 6, 8 and 12 nm and for encapsulated within polyethyleneimine (PEI) nanorods with core size ranging from 30 to 70 nm and high r_2 values in the interval of 312 to 608 mM^{-1} s^{-1}, respectively. Also, the increase of Ms value with the size increase is also observed for the described

systems above. When the r_2 relaxivity of the nanoparticles does not increase as the size does, the regime is called static dephasing regime (SDR) [81-83]. In SDR, nanoparticles create a magnetic field so strong that the T_2 relaxation process is barely affected by diffusion. Accordingly, it is predicted that a plateau of the maximum r_2 would appear. An example is water dispersible ferromagnetic iron oxide nanocubes encapsulated in DSPE-mPEG [84]. The increasing of core size from 22 to 28 nm leads to very slow decreasing of transverse relaxivity from 761 to 745 $mM^{-1}s^{-1}$. However, a further size increasing to 32, 42 and 49 nm leads to an abrupt reduction of r_2 values to 532, 343 and 296 $mM^{-1}s^{-1}$, respectively, and gaining more valuable leads to the aggregation of the nanoparticles. When the r_2 relaxivity decreases as the size increases the regime is called echo-limiting (ELR) [85]. The effect of a decline of the r_2 depends on the echo time, which is the time interval of the RF pulse that refocuses the nuclei spins. The nuclei spins are dephased when nanoparticles are too large; the fewer spins are refocused by the echo sequence, leading to decrease in the r_2 and the further aggregation, due to the ferrimagnetic dipole interactions.

A strategy to tune magnetic properties and to achieve a high transverse relaxivity is obtained by changing the shape of iron oxide nanoparticles, which affects the orientation of magnetic moments inside the particles as well as the dipolar interaction between IONPs. In a series of works different anisotropic IONPs (cubes, octahedras, disks, rings, octopod-like, rods) have been explored [34, 84, 90-96].

In comparison to spherical shape IONPs they are found to be more appropriate for MRI and hyperthermia applications because shape anisotropy offers higher surface area, larger effective diameter and induces localised magnetic field inhomogeneity around the particles. In the following sections, we provide an example of the recent studies of Mohapatra *et al.*, listed below. In Ref. [90] the team reports that 12 nm octahedral citrate coated USPIO with a core size of 12 nm exhibit higher relaxivity and specific absorption rate (SAR) than similar sized conventional spherical nanoparticles and commercial SPIONs. Increasing of core size from 6 to 12 nm leads to linear increasing of M_s values from 71 to 82 emu g^{-1}, r_2 values from 198 to 353 $mM^{-1}s^{-1}$ and SAR values from 163 to 275 W g^{-1}. In another recent work, Mohapatra *et al.* [80], propose a simple two-step reaction strategy for obtaining of encapsulated within polyethyleneimine Fe_3O_4 nanorods with a controllable core size of 30, 40, 50, 60 and 70 nm and excellent r_2 values of 312, 381, 427, 545 and 608 $mM^{-}1\ s^{-1}$, respectively. These values are much higher than those obtained for spherical IONP with similar material volume, being of 141 to 297 $mM^{-1}\ s^{-1}$ for 4 and 16 nm in size, although the last demonstrate higher magnetisation saturation. In the just-published paper, Beg *et al.* [34] show that porous single core

Fe_3O_4@SiO_2 nanorods of 520 nm length and 180 nm diameter reveal two-fold higher transverse relaxivity (~192 $mM^{-1}s^{-1}$) in comparison with commercial contrast agents. Also, the authors demonstrate their applicability as multifunctional nanoplatforms for magnetic theranostics. Although the promising reports for potential bioapplicability of anisotropic NPs, their advantages have not been well demonstrated in the literature because of challenges for their preparation, which have to accomplish the requirements for excellent shape and size control which means high reproducible production process.

Another method for improving the performance of SPIONs as negative contrast agents is by applying clusters of nanoparticles. In a very recent paper, Smith *et al.* [91] report how to control the self-assembly of SPIONs into worm-like superstructures using glycogen-like amphiphilic hyperbranched polyglycerols (HPGs) functionalized with peptides capable of binding to the defective vasculature. The SPIONs worm-like clusters possess a 3.5-fold higher T_2-weighted MR relaxivity than conventional SPIONs. According to the authors, the design principles exposed for these nanoprobes should be expanded to a range of different proper moieties for refining the diagnostics of other diseases. In recent work of Chen *et al.* [92] the team developed very stable nanoclusters of SPIONs with a controlled clustering structure using SPIO nanocrystals of size 8 nm and alkyl-modified polyethyleneimine. The advantages of the self-assembly of SPIO nanoclusters for universal cell labelling with MRI monitoring capability are presented. The nanoclusters show excellent performance on cellular uptake and cell labelling in a different type of cells, which are tracked by MRI with high sensitivity.

Many studies have been performed to investigate the MRI contrast efficiency of SPIONs and the effect of coatings in *in vivo* scenarios. The coating determines the overall size, stability and circulation lifetime of the nanoformulations, their distribution and fate in the organism, degradability and relaxivity. An example how optimisation of coating type and thickness could lead to high contrast *in vivo* imaging are shown in the works of Saraswathy *et al*. [93, 94]. The SPIONs with the same core size of 12 nm are coated with citrate or high molecular weight dextran. The coating thickness is optimised to achieve high r2/r1 ratio, being of 37.92 for 30 nm citrate coated SPIONs and 56.28 for 50 nm dextran coated SPIONs. The probes are used for MR imaging of liver fibrosis of male Wistar rats after injection of 2.17 mg/ml Fe/kg body weight. The post contrast T_2 weighted images 5 min after administration showed a hypointense liver with 39% and 55% decrease in the average MRI signal intensity for citrate and dextran coated SPIONs, respectively. The results indicate a higher hepatocellular uptake of dextran-SPIONs.

In recent work of Mishra *et al.* [95] 13 nm low molecular weight dextran coated USPIO nanoparticles (r_2/r_1 ratio of 4.92) are investigated for tumour detection, organs and whole mice body imaging. The signal started to drop remarkable in 1 hour after injection of nanoparticles (3.0 mg Fe/kg body weight), which continued up to 48 h, thus facilitating the distinction. For kidney and heart imaging maximum contrast is achieved at 24 h, while for solid tumours the maximum contrast is evident after 48 h.

Uchiyama *et al.* [96] prepared ethylamine-functionalized cationic USPIOs with high and lasting negative MRI contrast effect in the liver imaging of male Wistar rats and insignificant acute toxicity. The *in vivo* and *ex vivo* monitoring of nanoparticles biodistribution and dose effect (10 *vs.* 50 mg/kg) on clearance behaviour are investigated. The results showed that nanoparticles circulate freely throughout the vascular system, retent only in the liver, kidneys and bladder, and clearance process is dose-dependent.

Xie *et al*. [97] considered the impact of surface functionality and surface zeta potential on the contrast efficiency for *in vivo* vascular MR imaging of mouse brains, comparing 20 nm PEG/SPIONs-9 nm, 21 nm PEG/PEI coated SPIONs-10 nm and 24 nm Tween 80 coated PEG/PEI/SPIONs with dzeta potential of -5, 35 and 19 mV, respectively. All of the samples are with high r_2/r_1 ratio (up to 86.66) due to the anisotropic shapes of the core. After injection in Kunming mice (dose: 10 mg Fe/kg) all nanoprobes showed enhanced and long-lasting (24 h) T_2* MRI contrast effects in the mouse brains after 24h intravenous injection of the nanoparticles. However, the PEG/SPIONs exhibited stronger contrast-enhanced T_2* imaging effects than the others (especially in the first 30 min) and caused stronger reducing in T_2* values at different locations of the brain, implying that PEG/SPIONs were cleared more slowly by the mononuclear phagocytic system than the others.

In the study [98] Cano *et al.* apply the ligand-exchange method and amine-silane derivative triethoxy-silane (APTES) to produce hydrophilic 96.8 nm SPIONs with better structural stability, although with poor colloidal stability. To improve the previous outcomes, the authors applied partial PEGylation of silanized SPIONs [99]. They obtained that 47.6 nm ultrastable hydrophilic NPs have virtually no cytotoxicity and under a magnetic field of 1.5 and 9 T reveal a high r_2 value of 121.56 and 98.74 $mM^{-1}s^{-1}$, and a high r_2/r_1 ratio of 50.65 and 93.15, respectively. An excellent T_2 contrast *in vivo* imaging of the liver and the spleen is observed 1 hour after injection in female BALB/c mice even at the lowest dose (11mg Fe/kg). Moreover, it was shown that partial PEGylated SPIONs could be functionalized further by residual surface reactive amine groups offering a tunable platform for the development of smart diagnostic and therapeutic nanosystems.

Particular attention has to be paid to the work of Richard *et al* [38] devoted to the synthesis of size tunable USPIO for neoangiogenesis T_2 MRI contrasting. The team proposes to control the USPIO size to optimise MRI T_2 relaxation times, and neovascularization is targeted through the enhanced permeability and retention (EPR) effect. Using a nonaqueous sol-gel method assisted by microwave heating the USPIO nanoparticles with sizes 3, 6 and 9 nm are produced and coated with polyethylene glycol phosphonate moieties. The 3 nm-sized USPIO has dramatically low r_2 relaxivity whereas 9 nm-sized exhibits high r_2 value close to 200 $mM^{-1}s^{-1}$. An ischemia-reperfusion rat model has been chosen for neo-angiogenesis. Although 6 nm nanoparticles had a lower relaxivity than the 9 nm ones, the *in vivo* experiments show that the sharpest signal decrease is obtained for 6 nm USPIO, due to their better vascular circulation. Thus, the team demonstrates that the controlled nanoparticles size and the PEG passivation reduce the RES clearance, enhance their blood circulation time and permit ischemia targeting through the enhanced permeability and retention (EPR) effect.

The combination of nanoparticles with liposomes is an approach which is proven as an extremely elaborative in the fields of nanomedicine and nanobiotechnology. When liposomes encapsulate iron oxide nanoparticles the general term 'magnetoliposomes' (MLs) is used for the resulting colloidal structures [100]. MLs have been used as contrast agent for molecular imaging and as a theranostic tool [101-103], but mainly as an efficient MRI contrast agent with enhancing T_2 contrast [104] – Fig. 3

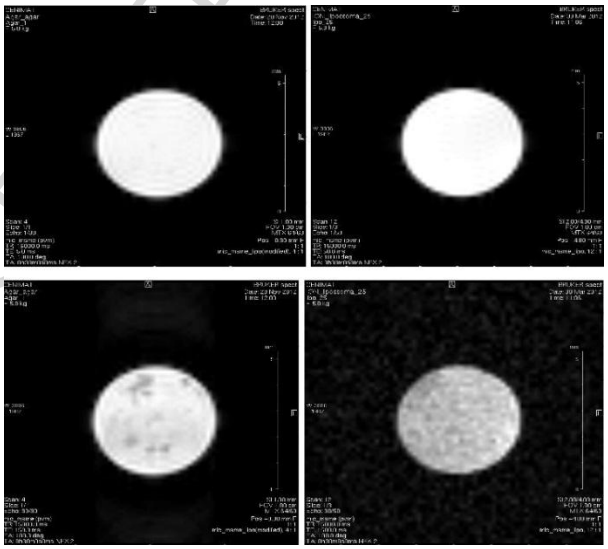

Fig. 3. First line: MRM axial image of the first echo for the aqueous phantom and for the SPC sample, respectively. Second line: MRM axial image of the 30 order echo, for the aqueous phantom and for the SPC sample, respectively - Reproduced from [104] with permission from the ELSEVIER.

Classical and extruded are two kinds of MLs depending on their structure. In the classical MLs, each iron oxide nanoparticle is surrounded by a bilayer of phospholipids. This kind of MLs was first prepared by De Cuyper *et al.* [105]. Different types of phosphatidylglycerols are used to form the liposomes. The whole size of the MLs is around 20 nm. For the preparation of classical MLs, magnetite nanoparticles were first stabilised with lauric acid and then sonicated phospholipid dispersions were added to the magnetite suspension. The second type extruded MLs, in which inside the lipid bilayer there are several iron oxide nanoparticles, they can act as an efficient MRI contrast agent with enhancing T_2 contrast. For these MLs, the ratios of the transverse and longitudinal magnetic resonance are between 6 and 18 $mM^{-1}\ s^{-1}$, which positions them among the best T_2 contrast agents. These MLs have been targeted successfully to solid tumours, and they led to a 52% contrast enhancement in the magnetically targeted tumour, while there was only 7% improvement in the nontargeted tumour [106]. In the work of Martínez-González et al. [107], the authors proposed sonication process applied to MRI response of hydrophobic or hydrophilic SPIONs loaded into MLs of different lipid composition. Liposomes were made of six formulations, differing in the fatty-acid chain length, the presence or absence of cholesterol (CHOL), and the presence or absence of negative charge (afforded by phosphatidylserine, (PS)). The relaxivity properties of such hybrid nanoparticles after sonification were determined at 7 T. The contrast is enhanced, and high values of r_2 are obtained when the hydrophobic nanoparticles are used.

In the work of Barbara *et al.* [108] the authors developed a new long circulating MLs which can be utilised as an MRI negative contrast agent for detection of liver ischemia–reperfusion injuries. The MLs are formed by encapsulation of a SPIONs covered with polyethylene glycol (PEGylated SPIONs) and were prepared by the dehydration–rehydration method followed by extrusion. In Fig. 4 is depicted a model of MLs formed by the encapsulation of a SPIONs suspension in a liposome is depicted. The MLs relaxivities r_1 and r_2 showed a minor effect on T_1 but a major effect on T_2. Thus the effectiveness as negative contrast agents of long circulating magnetoliposome, over approved clinical contrast agents such as Endorem and Sinerem, is proven.

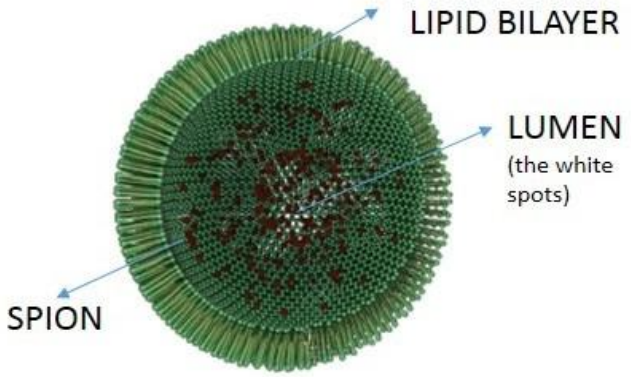

Fig. 4. Model of MLs formed by the encapsulation of a SPIONs suspension in a liposome.

2.1.3 Dual $T_1 - T_2$

The T_1–T_2 dualmodal strategy for MRI has attracted considerable interest because it can give highly accurate diagnostic information by the beneficial contrast effects in both T_1 imaging with high tissue resolution and T_2 imaging with high feasibility on detection of a lesion. Therefore, simultaneous achievements of positive and negative contrasts have been extensively followed to obtain complementary information on T_1-weighted MRI and T_2 -weighted MRI [109,110].

The application of the potential of SPIONs as a T_1 MRI contrast agent has been identified in the work of Chan *et al*. [111], where the size of SPIONs should be optimum (<5 nm) to achieve good T_1 contrast effect. Moreover, both T_1 and T_2 relaxations can be enriched in a single iron oxide nanoparticle by optimising their size, shape and surface coatings.

In an investigation of Zhou *et al.* [112] is shown that superparamagnetic nanoplates with (111) exposed facets have significant but interactional longitudinal and transverse relaxivities. By controlling structure and surface features, including morphology, exposed facets, and surface coating the authors demonstare that balance of T_1 and T_2 contrasts can be regulated.

In another investigation Ghobril *et al*. [113] showed that the dendron-modified SPIONs indicate better T_1 and T_2 contrasts, compared to commercial SPIONs used for MRI contrast [114, 115].

A simple way to construct T_1–T_2 dual-mode contrast agents is the conjugation of T_1 elements (e.g. Gd- or Mn-based chelates) and T_2 elements, as shown in the other work of Zhou *et al.* [116]. They

tailored iron oxide nanoparticles by including paramagnetic metal ions, such as Gd^{3+} and Mn^{2+}. The strong magnetic fields generated by T_2 contrast materials dislocate the T_1 relaxation processes, which results in a signal decrease. Therefore, the direct interaction of magnetic nanoparticles and paramagnetic ions should be avoided. Consequently, the separating layers, such as long PEG chains and/or silica shells, are required to control the magnetic coupling between T_1 and T_2 contrast materials. The r_1 relaxivity is dramatically increased from 2.0 to 32.5 $mM^{-1}s^{-1}$, while the r_2 relaxivity is ascetically decreased from 340 to 213 $mM^{-1}s^{-1}$ by increasing the thickness of the separating silica layer. [115, 117, 118]. In the Supplement information are summatised some results based on dual T_1-T_2 modalities presented like Table 2.

2.2. Combined Multimodal MR Imaging Agents –

Multimodality molecular imaging is now playing an essential role in the biomedical research. Multimodality imaging is emerging as a technology that utilises the strengths of different modalities and yields a combined imaging platform with benefits superior to those of any of its individual components. The commonly used clinical imaging modalities include optical imaging, X-ray computed tomography (CT), MRI, positron emission tomography (PET), single-photon emission CT (SPECT) and ultrasound imaging (UI). The advantages and disadvantages of these diagnostic technics are described elsewhere [119-123].

For example, MRI and CT have high spatial resolution and can provide detailed anatomical information, but they lack sensitivity. The PET and SPECT enable high sensitivity of monitoring metabolic pathways and ligand-targeted information, but have limited spatial resolution and cannot provide anatomical information. The optical imaging (e.g. fluorescence) is a selective, high-contrast method, which provides real-time guidance, and the same time is less costly and widely available [124]. However, it had qualitative nature and limited tissue penetration. On the other hand, a relatively new photoacoustic tomography (a hybrid modality), based on the use of laser-generated ultrasound offers a deep tissue penetration [125]. The improvement of diagnostics or guidance can be reached by using two or more techniques simultaneously which can provide more accurate and reliable data than when single imaging modality is used through analysis of complementary, co-registered, and data-rich images [126]. For example, the first fused PET/CT instrument was available commercially in 2001[127]. Moreover, the first commercial PET/MRI prototype was presented in 2007 [128]. For combined multimodal modalities, the use of multifunctional nanoparticles is crucial because the corresponding information can be provided with a single injection of functionalized contrast agent. The T_1 and T_2-contrast enhancement produced by SPIONs and the potentials for their functionalization with

radioisotope(s), biomarker(s), optical active molecule(s), drug(s) offer the opportunity to combine various modalities, such as PET/MRI, SPECT/MRI, PET/MR/optical imaging and etc. The strategies for engineering of magnetic nanoparticles and their ability in multimodal imaging are reviewed through the years, and some of the recently published works as follows [129-132].The examples given below are focused mainly on radiolabeled iron oxide nanoparticles

The other exampales based on multimodal imaging probes on SPIONs are summarised in Table 2 and presented in the Supplemental information section.

A common approach for radiolabeling of SPIONs is to attach isotopes onto the surface through chelating ligands or by passive adsorption. However, the process and further purification are complicated and relatively slow, and the stability of chelated radionuclide *in vivo* is often undefined [133, 134]. In fact, other approaches are now being explored: incorporation of radioisotopes into the nanoparticle core and chelator-free labelling procedures

^{99m}Tc or ^{64}Cu labelled bifunctional bisphosphonate-based chelators (BP) were used by Rosales *et al.* [135, 136] to bind a PET isotope and inorganic surface of dextran coated SPIONs (Endorem/Feridex). The *in vivo* MRI - nanoSPECT-CT [135] and PET–MR [136] imaging revealed the bimodal imaging capabilities and excellent stability of these nanoparticles. ^{89}Zr-labeled ferumoxytol (via coordination with desferrioxamine-DFO) was used for PET-MRI mapping of tumor-drained lymph nodes (LN) in mice [137].

A highly specific chelator-free approach for labelling of SPIONs was presented by Chen *et al.* [138]. The PAA coated SPIONs were labelled with radioarsenic nuclides *As (*=71, 72, 74, 76) and PEGylated further for increasing theirs *in vivo* stability. The team presents also a chelator free method for ^{69}Ge labelling of SPIONs [139]. The *As-SPION@PEG and intrinsically labelled ^{69}Ge-SPION@PEG nanoparticles were used for PET/MR dual-modality sentinel lymph nodes mapping. A new reaction for chelate-free, heat-induced metal ion binding and radiolabeling of USPIOs (ferumoxytol) was proposed recently by Boros *et al.* [140]. The authors demonstrated that high efficient labelling of metal-based nanoparticles with different isotopes, such as ^{89}Zr, ^{64}Cu, ^{111}In could be achieved under the similar reaction conditions. ^{89}Zr labelled ferumoxytol was tested for *in vivo* PET/CT imaging in mice and parallel for biodistribution. According to the authors, this chelate-free labelling method can be employed to facilitate clinical translation of a new class of multimodality PET/MRI radiotracers.

A multi-step procedure for the chelate-free synthesis of ^{68}Ga labelled nanorods for PET/T_2-MR multimodal imaging was reported by Burke *et al.* [141]. Siloxane polyethylene glycol derivative was

used for obtaining of PEG-coated iron oxide nanorods, preliminary synthesised. The presence of silica allowed further chelate-free labelling with ^{68}Ga due to the formation of Ga–O–Si bonds. The biodistribution was studied *in vivo*, and the stability of nanoradiotracers was proofed by *in vivo* and *ex vivo* analyses.

A challenge to labelled SPIONs with short-lived radioisotopes in one-step procedure was overcome by Pellico *et al.* [142]. The authors reported extremely fast and reproducible microwave synthesis (MWS) which allowed production of dextran coated extremely small (2.5 nm) ^{68}Ga core-doped iron oxide nanoparticles with high radiolabeling yield. Also, the measured value for r_1 relaxivity is greater than that of clinically approved Gd-based positive contrast agents. The team also demonstrated the likely use of these radiotracers by their further coupling with RGD peptide via a homo-bifunctional linker. The ^{68}Ga-SPIONs and ^{68}Ga-SPIONs-RGD were evaluated in murine angiogenesis model by PET-T_1 weighted MR imaging. The biodistribution was monitored. It was established that presence of RGD peptide lead to accumulation in the tumour area of tumor-bearing mice and selectively integrin binding to angiogenic endothelial cells.

The T_1-weighted MRI-SPECT multimodal imaging was also shown in the well-known work of Sandiford *et al*. [60], based on ^{99m}Tc labelled USPIONs. The *in vivo* tests reveal their potential for MRI angiography due to the long blood circulation time and high signal enhancement.

^{99m}Tc labelled USPIONs, conjugated with c(RGD) peptide were obtained by Xue *et al*.[143] for dual-contrast (T_1/T_2) MR and dual-modality (SPECT-MR) imaging of tumour angiogenesis. 3.5 nm USPIONs were synthesised using polyol method, coated with COOH-PEG-NH_2, further conjugated with cRGD and labelled with ^{99m}Tc (via chelator). The measured r_1 value is higher than that of clinically approved Magnevist. The biodistribution *in vivo* and *ex vivo* were monitored. It was established that the nanoplatforms retained mainly in the liver, spleen and stomach. The tumour accumulation of ^{99m}Tc-USPION-RGD was also significant.

Dual-mode agents for ultrasound imaging and MRI are the object of interest in recent years [144-148]. Microbubbles (MBs) with a gas core that is stabilised by a shell prepared of proteins, lipids, or polymers are typically ultrasound contrast agents.

In the work of Sciallero *et al.* [149] to the external surface of polymer-shelled MBs were anchored with different densities of superparamagnetic iron oxide nanoparticles or like a second scenario were physically entrapped into the shell. Under selection of a proper condition, set-up parameters and variation in the SPIONs densities satisfactory detection of the contrast agent by using both UI and MRI was achieved. When the SPIONs density was increased, the MRI contrast improved,

while the UI contrast worsened due to the reduced elasticity of the MB shell. The MBs with SPIONs which are externally anchored provided improved performance than MBs entrapped into the shell SPIONs for both UI and MRI.

In the study of Teraphongphom *et al*. [150], the authors developed MBs by encapsulating nanoparticles including aqueous or organic quantum dots (QD), magnetic iron oxide nanoparticles or gold nanoparticles (AuNP) to create bimodality platforms in a manner that minimally compromised the performance of each imaging technique.

In the work of He *et al.* [147], they described the MBs ability to enhance UI and MRI image contrast. In this study, the authors synthesised MBs with a novel structure, which included a nitrogen gas core, a polymer shell, and SPIONs on the shell surfaces. The MBs with such structure applied to *in vitro* experiments provided both higher UI and MR enhancement than blank MBs without SPIONs and previously designed microbubbles where the SPIONs are embedded. Figure 5 represents the SEM and TEM characterization of microbubbles. SEM images showed that all microbubbles were spherical. Blank MBs surfaces were the smoothest, and SPIO-embedded MBs surfaces were coarser. TEM images showed the distributions of the nanoparticles. No nanoparticles could be observed from blank microbubble. On SPIO-coated microbubble's surface nanoparticles were randomly distributed, but for SPIO-embedded MBs, the nanoparticles were mostly distributed in the shell, and only a small number were adsorbed on the surface (Fig. 5).

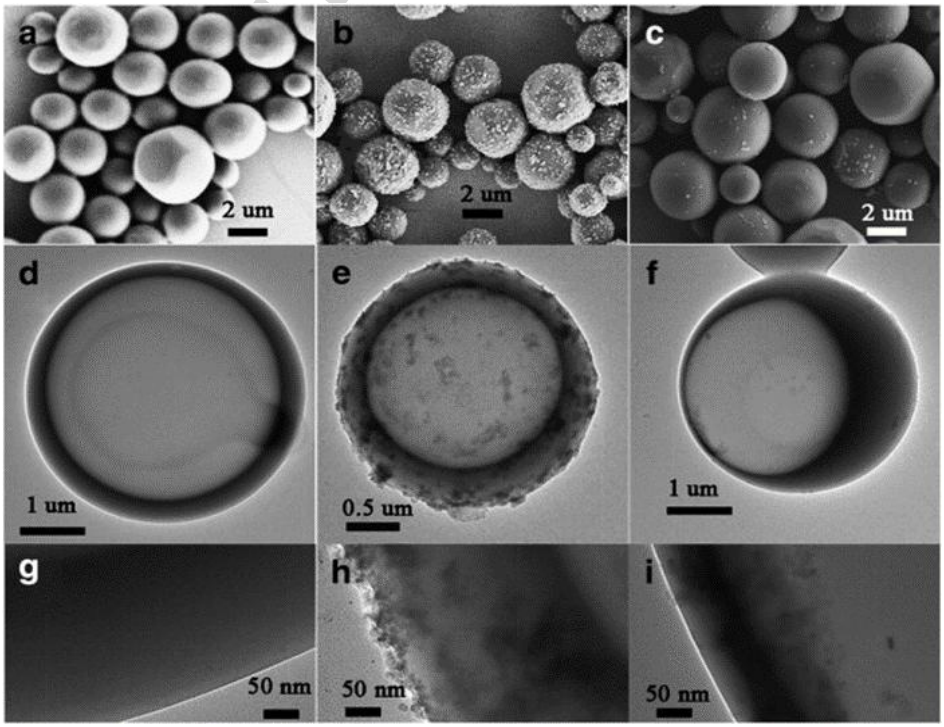

Fig. 5. SEM images of (a) blank microbubbles, (b) SPIO-coated microbubbles, (c) SPIO-embedded microbubbles, TEM images of (d) blank microbubble, (e) SPIO-coated microbubble, (f) SPIO-embedded microbubble, (g–i) are partially enlarged images of (d–f). Reproduced from [147] with permission from the ELSEVIER.

The authors conclude that some SPIONs-loaded MBs have been developed as contrast agents for UI/MR dual-modality imaging investigations. However, the disadvantage of such type of UI/MRI contrast agents were reported like a low degradation in the body [151, 152]. A contrast agent for UI/MRI dual-modality imaging with biodegradable multifunctional nanoscale particles is desired, and the number of such systems is increasing in the last years. The group of Yang *et al.* [153] developed a new class biodegradable yolk-shell magnetic microspheres for UI/MRI dual-modality imaging. The nanosystem contains a magnetic core of Fe_3O_4 nanocluster stabilised by poly(γ-glutamic acid) (PGA) and functional shell of disulphide cross-linkage biodegradable poly(methacrylic acid (PMAA). The authors handled perfluorohexane (PFH) like an ultrasound-sensitive object into the inner cavities of yolk-shell microspheres to gain ultrasound imaging signal. The yolk-shell microspheres attend as perfect contrast agents for UI/MR dual-modality imaging. The entire process of fabricating biodegradable Fe_3O_4@PMAA microspheres is demonstrated in Fig. 6.

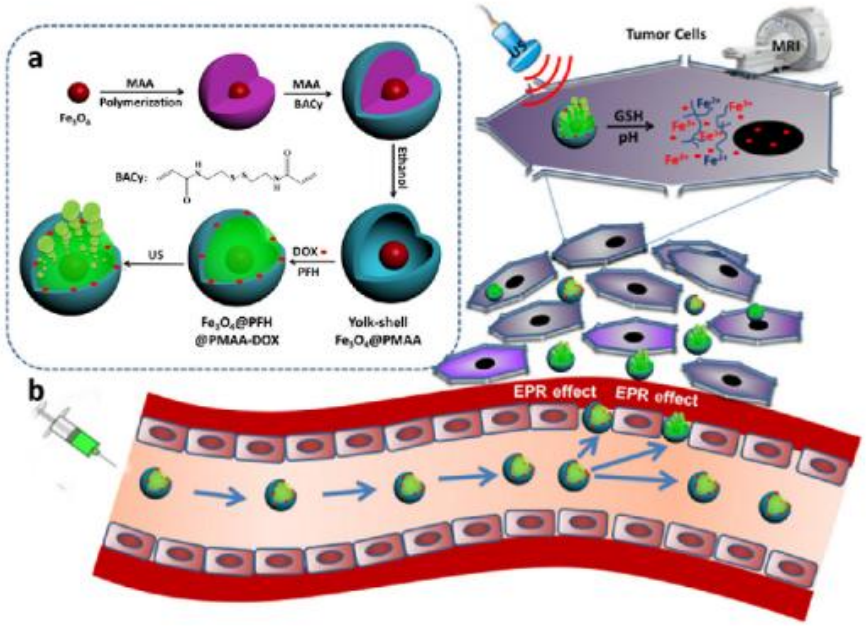

Fig. 6. (a) Schematic illustration of the preparation of uniform biodegradable yolk-shell Fe_3O_4@PFH@PMAA-DOX microspheres; (b) Schematic setup for US and MRIdual-modality imaging and drug delivery system using Fe_3O_4@PFH@PMAA-DOX microspheres. Reproduced from [153] with permission from the ELSEVIER.

The review stresses on the MLs like another object that can serve as a multimodality contrast agent. The flexible nature of the ML coatings, together with the simple production procedure, allows fast and easy modification of the surface and offers many exciting applications as multimodal contrast agents. In the recent work of Malinge *et al.* [154], they describe a new liposomal formulation enabling PET and magnetic resonance MR imaging. Compared to other protocols outlined in the literature [138, 155], the proposed process by the team of Malinge is rapid and simple to use in clinical and preclinical laboratories practice. The bimodality is achieved by coupling ^{68}Ga-based radiotracer on the magnetic liposomes bilayer. The two new phospholipids were synthesised, ^{68}Ga (DSPE-PEG-NODA) with a specific chelator and the second (DSPE-PEG-NODA-Glu) with a glucose moiety. The liposomes were produced according to a fast and safe process with a high radiolabeling yield. MR and PET imaging were performed on mice bearing human glioblastoma tumours (U87MG) after *in vivo* injection. The MR and PET imaging is created by the accumulation of the liposomes in solid tumour.

To achieve more accurate diagnosis *in vivo* much comprehensive information is required, so the interest in developing of nanoprobes for tri and higher mode imaging is grown in the latest years. The examples for PET, SPECT-MRI-optical multimodal imaging could be found elsewhere in the literature so that we will focus on the recent examples with other modality– photoacoustic tomography (PAT). PAT is a relatively new hybrid modality with potential for several clinical applications, including imaging of cancer [156] and vasculature [157]. With deep tissue penetration PAT is excellent complementary imaging techniques for PET and also could be combined with photothermal imaging (PTI).

Double-PEGylated reduced graphene oxide (RGO) nanosheets anchored with iron oxide nanoparticles and labelled with ^{64}Cu via NOTA-chelator were used for PET-MR-PAT imaging [158]. The nanoconjugates obtained exhibited a high stability due to the second PEG-layer, prolonged blood circulation half-life and remarkable tumour accumulation. PEGylated ^{64}Cu-MoS_2-IONPs were developed and tested *in vivo* for triple-modal PET-MRI-PAT imaging-guided cancer therapy [159]. The efficient tumour retention of nanoradiotracer was established and the conducted photothermal therapy showed an effective tumour ablation. The synergetic benefit of multimodality by providing of imaging-guided photothermal therapy was also demonstrated by Lin *et al*. [160]. The authors reported an innovative procedure for obtaining of new type IONPs-based contrast agents (magnetic melanin nanoparticles) and their labelling with ^{64}Cu by biomimetic synthesis method. The possibility of the prepared nanoparticles to serve as a versatile biomimetic theranostic agent for PET-MR-PAT-PT multimodal-imaging-conducted cancer photothermal therapy was shown.

The magnetic nanoparticle-based multimodal imaging approaches hold the new capacity to sheltered enhanced imaging sensitivity and precision for a better understanding of biological systems and accurate imaging of biological targets.

2.Therapeutic platform based on magnetic nanoparticles -

2.1.Magnetothermal Treatment

Although the magnetothermal effect values of SPIONs increase as the frequency (f) and/ or the amplitude (H) of the magnetic field increases, it is recommended that the product of the frequency and the amplitude (H_f) should be smaller than 5×10^9 A m^{-1} s^{-1} for the safety of patient [161, 162]. For example, Megaforce's NanoTherm therapy, which has been approved in Europe for the treatment of brain tumours, uses the magnetic field at a frequency of 100 kHz and field amplitudes in the 2−15 kA m^{-1} range where the product Hf is below the threshold [163]. Significant efforts are devoted to maximising heating efficiency (i.e., excellent SLP) of nanoparticles in a given frequency/amplitude of magnetic field and to improve an external magnetic field setup that generates a focused AMF. In a traditional magnet configuration, magnetic nanoparticles dispersed in any tissues including normal tissues are equally heated because AMF is nonselectively applied inside the solenoid. This unwanted and non-selective heating is the most serious shortcoming in this type of technique. Recent studies on the application of a static magnetic field show the potential of AMF focusing [164, 165]. The focusing position can also be changed by giving different amplitudes of direct current to the solenoids.

Temperature measurements with high resolution and accuracy are critical in nanoparticle-based thermal therapeutic applications [166, 167]. The optical method is of substantial importance to quantify magnetic nanoparticles local temperature [168-172].

Magnetic nanoparticles linked with fluorescent dyes such as a DyLight549 fluorophore or coated with a thermoresponsive fluorescence polymer such as poly(N-isopropylacrylamide-fluorescent modified acrylamide) (pNIPAM-co-FMA) changes their fluorescence intensity depending on the surrounding temperature. Absolute temperature detection is also possible. In a study with maghemite nanoparticles coated with rare earth metal chelates (e.g., Tb^{3+} and Eu^{3+}) in a silica shell was found that the emission from Tb^{3+} chelates is temperature-dependent, while that of Eu^{3+} chelates remains constant for the same temperature region. The determination of the ratio of Tb^{3+} over Eu^{3+} emission allows the absolute temperature measurement. In another study [171] subnanometer scale temperature gradient profile versus the distance from the surface of the magnetic nanoparticles was demonstrated by a thermolabile azo-linker, 2,2′-azobis[N-(2-carboxyethyl)-2-methylpropion-amide], functionalized with

fluorescein amine. Another similar example is the utilisation of a rigid DNA double helix structure [170]. The 12 nm core iron oxide nanoparticles stabilised with 2 nm thick amphiphilic polymer are conjugated with single-stranded DNA and subsequently hybridised with fluorophore-modified DNA having lengths of 3.0, 3.3, and 3.6 nm, each with different melting temperature. After AMF application, local temperatures at three different distances from the surface of the nanoparticles (i.e., 5.0, 5.3, and 5.6 nm) are determined by correlating the denaturation profiles of the DNA.

Despite the satisfactory spatial resolution, high-cost and the requirement of significant facility investment are limitations. That is why ultrasound seems to be an alternative imaging temperature monitoring due to the low price and positive response [173]. Among others, attenuation is known to be one of the most promising parameters and has been widely used in ultrasound thermometry. Attenuation is the amount of energy lost due to the reflection, scattering, or absorption of energy when ultrasound passes through a medium. Many studies have shown that the attenuation rate increases at high temperature.

2.2.Thermal Ablation.

Exposure to high temperature above 50 °C causes cancer cell death [166, 167]. The application of magnetic nanoparticles seems to be an acceptable alternative due to their perspective properties. Once the magnetic nanoparticles are administrated, the nanoparticles can be preferentially accumulated at the tumour site. Therefore, the concurrent external magnetic field application can ablate the tumour in a remote and noninvasive manner. One *in vivo* animal feasibility test was carried out using human breast adenocarcinomas-implanted immunodeficient mice [174]. After intratumoral injection of iron oxide nanoparticles, the mice are exposed to an AMF for 4 min (amplitude 6.5 kA m^{-1}; frequency 400 kHz). In the experiment the temperature is increased up to 73 °C. Histologic tests indicate early stages of coagulation necrosis in the tumour tissue. Indeed, these nanoparticles can create a localised hot spot. It could kill tumour cells. However, the poor energy-transfer efficiency of the iron oxide nanoparticles (i.e., low SLP) as a mediator presents could leave to serious problems. In the work of Lee *et al.* [175] the authors developed a core−shell magnetic nanoparticle, $CoFe_2O_4$@$MnFe_2O_4$, with a very high SLP of 2280 W $g^{-1}_{(magnetic\ atom)}$. A small amount (75 μg) of 15 nm $CoFe_2O_4$@$MnFe_2O_4$ nanoparticles dispersed in normal saline (50 μL) are injected into a U87MG human brain tumour (100 mm^3) in mice; then, an AMF of 500 kHz at 37.3 kA m^{-1} is applied for 10 min. After 18 days, the tumour treated with the core−shell nanoparticles is eliminated. For the case of treated mice with Feridex possessing low SLP of 115 W $g^{-1}_{(magnetic\ atom)}$, the tumour size increases by 9-fold in 18 days and its growth behaviour

is similar to that of the untreated control mice group. Initially, the tumours show a stage of regression (for the doxorubicin-treated group), but they recover in a much larger size.

2.3. Apoptotic Hyperthermia.

Although the use of thermal ablation has the advantage of quick tumour removal, the surrounding healthy tissues are possibly damaged and cannot be preserved at the high temperatures needed to kill the surrounding cancer cells. A lower-temperature window between 42° and 45°C can offer the possibility of destroying the cancer cells preferentially [176, 177], which is called hyperthermia [163, 178] - (Fig. 7). A temperature below 45°C induces apoptotic cell death, which is a more benign form of the "programmed" cell death compared to necrosis [1179, 180]. Phagocytosis removes cells dying during the apoptosis without impact on the neighbouring healthy cells [181, 182]. Many magnetic nanoparticles, including Fe_2O_3 coated with stabilisers and Fe_3O_4 encapsulated in cationic liposomes, have been tested for magnetic hyperthermia and this form of hyperthermia is clinically approved in Europe for the treatment of glioblastoma [183].

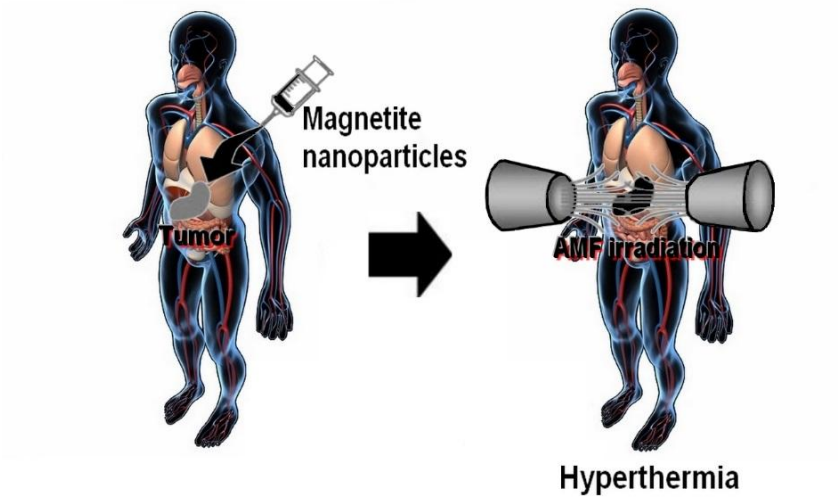

Fig. 7. Therapeutic strategy using magnetic particles - hyperthermia

If superparamagnetic nanoparticles are considered, many approaches for magnetic hyperthermia, which is self-controlled heat mediator based on ferromagnetic nanoparticles with optimised Curie temperature (T_c) could be cited [18-190].

As known, magnetic materials could change magnetic properties above T_c and it prevents the conversion of electromagnetic energy into heat. Therefore, T_c appears to be the maximum temperature

which magnetic nanoparticles could reach. Controlling T_c can be an effective way to prevent overheating.

Recent studies show ways to improve the magnetic hyperthermia efficacy, and the first approach is targeted intracellular hyperthermia. Surface epidermal growth factor receptors (EGF) in cancer cells were targeted by carboxymethyldextran-coated iron oxide nanoparticles conjugated with EGF. If the intracellular hyperthermia effect is recorded at different specific absorption rates (SAR), it could be observed that at a high SAR, the survival factor of cancer cells treated with the magnetic nanoparticles and magnetic field decreases by 0.06% without a noticeable rise in temperature [191]. Another example is the folic acid (FA), and PEG-functionalized superparamagnetic nanoparticle clusters (FA-PEG-SPION NCs) [192]. The FA-PEG-SPION NCs, produced via the thiolene click reaction between allyl-SPIONs and thiol of FA-functionalized PEG, are intravenously injected, and AMF (8 kA m^{-1}, 230 kHz) is applied to tumor-bearing mice to inhibit tumour growth significantly.

DeNardo *et al.* [193] proposed an approach which demonstrated for heat shock protein (Hsp) 90 targeted hyperthermia. The thermal tolerance is related to Hsps, known to protect cells from apoptosis. In the experiments, geldanamycin (GM), known as Hsp90 inhibitor, is combined to 15 nm $Zn_{0.4}Fe_{2.6}O_4$ nanoparticles by thermosensitive 4,4′-azobis(4-cyanovaleric acid).The magnetic nanoparticles generate the heat necessary for MDA-MB-231 cancer cell death and also release GM by thermal cleavage of the azo bond in the presence of an AMF. The released GM efficiently blocks Hsp90's chaperonic function in cell survival, and the efficiency of hyperthermia-mediated apoptosis is significantly enhanced. While the conventional magnetic hyperthermia at 43°C for 80 min induces only 25% cell death, this newly developed magnetic nanoparticle system significantly increases the cell death to 89% in 60 min and completely removes all the cancer cells in 70 min. *In vivo* efficiency of this method is also validated where the breast cancer xenografted in mice is completely removed with the GM-linked magnetic nanoparticles, while the conventional magnetic nanoparticles show a 2.5-fold increase in the tumour volume on day 14 after a single hyperthermia treatment.

The magnetic nanoparticle-based thermal treatment possesses serious advantages due to the possibility for synergistic combination with treatments like chemotherapy, radiation therapy, gene therapy, and photodynamic therapy. For instance, hyperthermia combined with radiation or gene therapy is more effective than either hyperthermia or radiation/gene therapy alone because of the complementary mechanisms of cell death. One good example is the application of 20 nm dextran-coated iron oxide nanoparticles in the treatment of prostate cancer [194]. The exposure of the nanoparticle-treated cancer cells to AMF followed by radiation results in a significant cell death.

Another example is 23 nm $ZnFe_2O_4$ magnetic nanoparticles complexed with lethal-7a miRNA using branched PEI via a layer-by-layer approach.

Through the increased retention of the magnetic nanoparticles in the tumour sites the antibody-labeled magnetic nanoparticles show enhanced efficacy as a result of tumour targeting, magnetic hyperthermia, and radiation, therapy and chemotherapy for the therapeutic efficacy enhancement.

3. Magnetic hyperthermia therapy

Hyperthermia therapy (HTP) is a heat induced malignant cancer treatment where SPIONs serve as heat producers. To provoke a treatment effect SPIONs are introduced near to the cancer tumour location by the use of magnetic targeting. An alternating magnetic field (AMF) is applied for a specified period to produce heat for initiating apoptosis in cancer cells. Optimal results could be achieved by controlling the size, shape, crystallinity, magnetic properties of SPIONs and parameters of the applied AMF. The effect of the therapy is assessed by the specific absorption rate (estimate of the conversion of the AMF into heat) Cervadoro *et al.* [195] reported that the relaxations required for inducing heat from SPIONs (5, 7 and 14 nm sized) started to take place at a frequency range i.e. less than 1 MHz and ending above this frequency range when tested for wide range of frequencies (up to 30 MHz). In a similar fashion as reported by Lartigue *et al.* [30], multicore magnetic nanoparticles exhibited high SAR value of almost 2000 W g^{-1} (applied field of 29 kA m^{-1} and frequency of 520 kHz) with an increase in temperature rate of 1.04 $^{\circ}C$ s^{-1} for an iron concentration of 0.087 M. As indicated by Fantechi *et al.*[196], doping of SPIONs with other metal atoms (like manganese) can improve the hyperthermia activity of magnetic nanoparticles. However, copper (5%, 10%, 15%,) doped iron oxide core (7 nm) resulted in very low SAR values, owing to the lower size of ferritin molecules coated magnetic core.

The attractive therapeutic effects of SPIONs are demonstrated in various *in vitro* and *in vivo* scenarios. For example, 14 nm magnetic nanoclusters (with SAR value of 500 W g^{-1}) killed almost 74% of MCF-7 cancer cells in *in vitro* conditions, where a therapeutic temperature of 45 ^{0}C for 1 h was maintained [197]. The cell viability of HeLa cells was reduced to 42% as these cells were exposed to a temperature of 43°C (for 1000 s) which was induced by applying an alternating magnetic field to silica-coated iron oxide nanoparticles [198]. In another study [199], the magnetic nanoparticles reveal their *in vitro* hyperthermia levels (42–45°C) in less than 200 s at a frequency of 26.48 kA m^{-1}, in experiments with three different cancer cell lines (DA3, MCF-7 and HeLa). It was proven that the induction of apoptosis in cancer cells through magnetic nanoparticles increases with an increase in the

concentration/quantity and the size of these nanoparticles. Jadhav *et al.* [200] reported that the induction of apoptosis process in WEHI-164 tumour cells increased near to 80% when the quantity of sodium carbonate-stabilized-oleic acid-functionalized magnetic nanoparticles was increased from 0.22 mg to 0.44 mg. Khandhar *et al.* [201] compared the survival rate of Jurkat cells for different Fe concentrations of magnetic nanoparticles. In a new study, polymer stabilized-iron oxide-graphene nanocomposite attained a heat of 42°C for a concentration of 2.5 mg/ml within 15 min of application of AMF at 418 Oe, where −40 ± 4% and −76 ± 3% of cell death was observed after 4 and 8 h incubation of nanocomposites with HeLa cells [202].

Hayashi *et al.* [192] reported that the exposure of magnetic nanoclusters to AMF intensity of 8 kA m^{-1} and frequency of 230 kHz decreased the size of the tumor in female CB17/Icr-Prkdcscid mice, where the folic acid attached to magnetic nanoclusters (with an average SAR value of 248 W g^{-1}) were injected intravenously. A significant temperature increase was observed in comparison to the surrounding tissues. Moreover, the volume of the tumour decreased to one-tenth times of the tumour in control mice after 35 days of treatment, where the life-span of hyperthermia treated mice extended by four weeks. In the study of Basel *et al.* [203] intraperitoneally injected magnetic nanoparticles helped in the reduction of tumour created via injection of Pan02 cells into C57BL/6 mice after getting exposed to 15–20 min of AMF, thereby improved the life expectancy rate of mice by 31%. In another case, the volume of SCCVII squamous cell carcinoma induced in mice was comparatively reduced through magnetic nanoparticles at an appropriate intravenous dose and applied a field of 38 kA m^{-1} at 980 kHz [204, 205]. In a similar fashion, polypyrrole coated Fe_3O_4 nanoparticles showed an SAR value of 487 W/g, where the nanoparticles considerably inhibited the growth of myeloma tumour induced in Female CB17/Icr-Prkdcscid mice but completely when a combination of Fe_3O_4 nanoparticles and a chemotherapeutic drug at a quantity of 5 mg/kg was used for cancer therapy.

In a recent study [206] a novel injectable liquid to the solid phase transitional magnetic material, polymethylmethacrylate (PMMA)–Fe_3O_4, designed for highly efficient magnetic hyperthermia ablation of tumours was developed. The morphology characterization, magnetic properties and heating efficiency of PMMA–Fe_3O_4 were studied. The Fe_3O_4 particles were evenly distributed in the PMMA and the hysteresis curve of Fe_3O_4 and PMMA–Fe_3O_4 indicated that they were magnetic materials. When exposed to an alternating current magnetic field *in vitro* the magnetic PMMA–Fe_3O_4 generated heat. The increased temperature of excised bovine liver was positively correlated to the iron content and time, which suggested that the temperature inside the tumour was controllable. In the *in vivo* animal experiments a MB-231 breast cancer xenograft model was obtained

in nude mice. In this tumour model PMMA–Fe_3O_4 was injected precisely using guided ultrasound imaging which was proven by the computer tomography images. The tumours were completely ablated by a dose of 0.1 ml, 10% PMMA–Fe_3O_4 with 180 s exposure time in the magnetic field. The results demonstrated that PMMA–Fe_3O_4 was an excellent magnetic material for the localised magnetic hyperthermia ablation of tumours.

The study presented by Grillo *et al*.[207] were based on the synthesis of sub-micrometer and magnetic polymer nanocomposite capsules (MPNCs) employing the oil-in-water emulsion/solvent evaporation method. The MPNCs showed a significant increase in the particle size from 400 - 800 nm as the magnetic loading in the organic–inorganic hybrids increases from 1.0% to 10%. The MPNCs presented high incorporation efficiency of Fe_3O_4@OA nanoparticles, excellent colloidal stability, and super-paramagnetic properties. Interestingly, electron microscopy results showed that the Fe_3O_4@OA nanoparticles were preferentially located at the surface of the capsules. Evaluation of the magnetic properties revealed that the saturation magnetisation and the blocking temperature of the MPNCs samples increased as a function of the Fe_3O_4@OA loading. All the MPNCs were heated when subjected to MH and demonstrate real specific absorption rates. When the MPNCs-cell interaction was tested lower cellular toxicity to healthy cells compared to cancer cells was indicated by MPNCs. These findings help in understanding the relationships between magnetic nanoparticles and polymeric capsules opening perspectives for their potential clinical uses as simultaneous heating sources and imaging probes in MH and MRI, respectively.

In the work of Cristofolini *et al.* [208], the authors checked the applicability of magnetic nanocapsules (polyelectrolytes and magnetic Fe_3O_4 nanoparticles) to hyperthermia treatment. The hyperthermia effect was demonstrated by applying the RF magnetic field with maximum fields up to 0.025 T and frequencies up to 430 kHz; they found sizable heating effects, with a heating rate up to 0.46°C min^{-1}. They also comment the effects of irradiation on capsules morphology that indicated their potential disruption use as nanocarriers of drugs that can be locally released on demand.

MLs hybrid nanoparticles made of SPIONs coated with liposomes are emerging as the new class of bio-nanomaterials due to their potential applications in hyperthermia cancer therapy. The applicability of SPIONs for therapeutic purposes is increased when liposomes coat them. The hyperthermia treatment is based on the fact that SPIONs, when subjected to an oscillating magnetic field, generate heat and thus can kill tumour cells which are more sensitive to a temperature above 41°C than the normal cells. Magnetoliposomes are very useful for hyperthermic applications. It is related to their properties as bilayer systems (high temperature dependence leading to corresponding

temperature response). The SPIONs of this kind are stable (surface-attached oleate molecule and dispersion in organic solvent ensure this stability). The transfer to aqueous media is also possible. This phase transfer relies on NP surface derivatization strategies replacing the originally grafted hydrophobic molecule with hydrophilic compounds or direct functionalization of the surface-grafted hydrophobic molecules themselves [209]. Surface chemistry not only determines the colloidal stability of the NPs but also their association to the liposome, i.e. whether they will be embedded in the hydrophobic bilayer or within the hydrophilic lumen [210].

Di Corato *et al.* [211] designed an approach to effective tumour therapy by creating a system based on dually loaded hybrid liposomes. The aqueous core includes loaded with iron oxide nanoparticles. The lipid bilayer, on the other hand, is equipped with a photosensitizer payload. This combination leads to the generation of singlet oxygen under laser excitation and heat production under alternating magnetic field stimulation. Thus, the photodynamic therapy is readily combined with magnetic hyperthermia. These liposomes address both therapeutic agents within tumour cells, and the combined PDT/MHT treatment resulted in total cancer cell death *in vitro* while total solid-tumor ablation was achieved in an *in vivo* rodent model.

An excellent review dealing with recent advances in the application of SPIONs for *in vitro* and *in vivo* cancer theranostic was published by Kandasami and Maity [212].

5. Toxicity

Iron oxide nanoparticles have proven to be convenient in a wide-ranging of applications besides its original design intention as high-performance seals in space application. Iron oxide nanoparticles have frequently been used for cells labelling and for *in vitro* separation and sorting and *in vivo* tracking magnetically. Although, the general assumption that IONPs are biocompatible, the data presented in the literature are sometimes conflicting. The most frequently suggested description of IONP toxicity encompasses the generation of reactive oxygen species (ROS), which causes lipid peroxidation, disrupting the phospholipid-bilayer membrane, resulting in cell death. IONPs are efficiently internalised by cells *via* endocytosis because of their nanoscale size. The IONPs are degraded by hydrolysis into iron ions within acidic organelles such as endosomes or lysosomes. The free iron ions are then transported through the organelle membranes through the divalent metal transporter-1 (DMT_1) into the cytosol, where they undergo the Fenton reaction with the mitochondrial hydrogen peroxide (H_2O_2) to form hydroxyl radicals (•OH), a highly reactive ROS.

In the very recent work of Huang *et al.* [213], they posed hypotheses for toxicity of IONPs that are internalised into cells by endocytosis, depending on the pH of the environment to which the particles are exposed during their endocytotic transportation. IONP toxicity consideration is a necessary is we want to design and use IONP nanosystems with a vast range of clinical applications. The authors claimed a thermo-responsive liposomal system that contained ammonium bicarbonate (ABC, NH_4HCO_3) for localised drug delivery (Fig. 8). At an elevated temperature (42°C), the decomposition of ABC generates CO_2 bubbles that create permeable defects in the lipid bilayer of the liposomes. The proposed model revealed that the local environment in cellular organelles, in which the pH-dependent degradation of IONPs and the release of iron ions occur, critically affects the amount of intracellular generated ROS, which causes lipid peroxidation and eventual cell mortality. In the literature concerning IONP toxicity [214-217] we observed contradictory results. Usually, toxicity could be severely related to the intracellular transport environment of the IONPs. For applications in cancer diagnosis and cell separation/sorting and tracking, the early endosomal escape of IONPs is crucial to preventing toxicity toward target cells. Conversely, the direct exposure of IONPs in lysosomes can significantly elevate their intracellular toxicity, possibly by improving their effectiveness in cancer treatment.

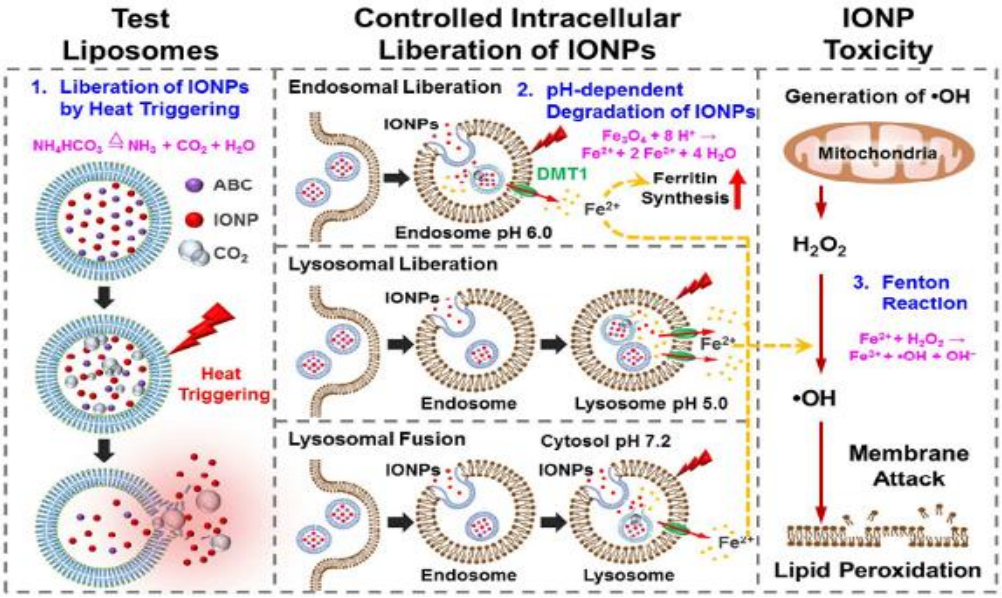

Fig. 8. Schematic illustrations showing the structure of thermoresponsive bubble-generating liposomal system and its process of spatially precise, controlled intracellular liberation of IONPs in specific cellular organelles in various endocytotic stages. The degradation of IONPs, release of iron ions, and subsequent reactive oxygen species (ROS) generation within cells are indicated. IONPs: iron oxide

nanoparticles; ABC: ammonium bicarbonate; DMT1: divalent metal transporter-1. Reproduced from [213] with permission from the American Chemical Society. Copyright 2017.

The SPIONs materials are relevant in a vast number of biomedical applications; the question is that this type of applications requires knowledge about the potential interaction between nanoparticles and biosystems. Unfortunately, the results obtained concern still a restricted number of materials and products. It is a general opinion that individual assessment is needed when hazardous impacts by nanomaterials are considered, and the primary concerns are related to the size of the particles, their surface charge and their unspecific protein absorption ability.

5.1. In vitro toxicity assessment

In various studies [218, 219] it is shown that different *in vitro* toxicity tests used for determination of the toxicity of other that SPIONs nanoparticles could be applied to SPIONs as well, e.g. the viability of cells, i.e., cytotoxicity, oxidative stress, inflammatory reactions, and genotoxicity. *In vitro* nanotoxicity assays of SPIONS could be described shortly as follows [220]:

- Nanoparticles cell interactions (including cell morphology and attachment of nanoparticles to cell membrane and further uptake) to be transformed into cellular response signals (cell decay or cytotoxicity, metabolic activity, antioxidant production due to oxidative stress, inflammation, genotoxicity); the respective assays are *MTT Assay*, *PI Assay*, *BrdU Assay*, *LDH Assay* (checking mitochondrial activity, DNA staining, DNA replication staining and membrane integrity assessment, respectively).
- Nanoparticle cellular uptake was studied initially by Dextran-coated SPIONs as model systems [221-223]. It was found that different cells could be reliably labelled with SPIONs and further used for *in vivo* tracking procedures.

Initial information about significant toxicity in SPIONs was presented by Mueller *et al.* [224] more than 20 years ago. This was followed by several studies of Berry et al. as well as by Gupta *et al.* [225-228] showing that uncoated or dextran-coated SPIONs or bare SPIONs could cause varying degrees of cell death, vacuole formation and disruptions of the skeleton of dermal fibroblasts cytotoxicity and cytoskeletal damage. The coating of SPIONs by different proteins (lactoferrin, ceruloplasmin) has shown that the cell response could be modulated by the proper selection of surface. Later, van den Bos

et al. [229] demonstrated the toxic effect of Feridex material (dextran-coated SPIONs) in the case of macrophage exposure with decreased proliferation and cell death. Stroh *et al.* [230] have found that significant amount of SPIONs coated with citrate increase protein oxidation and oxidative stress.

An interesting aspect of the *in vitro* toxicity of SPIONs is the comparison between their toxic impact and the toxicity (cancerogenic effect) of asbestos nanoparticles as done in [231-233]. It was convincingly shown by transmission electron microscopy and toxicity assays that murine macrophage cells exposed to bare SPIONs showed cytotoxicities nearing 90% of the asbestos-treated cultures. The authors explain the possible role of Haber – Weiss reactions due to the more rapid uptake and transportation of nanoparticles through the cells as compared of those of bare ions [231]. Significant morphological effects but relatively low toxicity upon a neuroblastoma cell line by SPIONs is reported in [234]. Au et al. have studied the impact of a commercial material (NanoSonics (Blacksburg, VA) based on SPIONs upon astrocytes and have found detectable effects on the mitochondrial function and decreased cell viability [235]. In a similarly designed study [236] Pisanic *et al*. present a model cell system which response to the toxicity impact of SPIONs coated with dimercaptosuccinic acid. It was found that the particles show a dose-dependent diminishing ability of the cells to survive and keep normal biological functions and morphology.

It is proven that the surface coating of nanoparticles is of substantial importance for the stability, aggregate size and cellular interactions related to the SPIONs uptake in intercellular medium [237]. Diaz *et al.* [238] report on the uptake of SPIONs in relation to the cell type. The responses were entirely different indicating the role of the tested cell line. The same study shows that the number of particles per cell (not the concentration) might influence the response of the toxicological assay. It hinders the opportunity to find a direct relation between ROS production and cellular toxicity. For instance, in [239] is indicated that SPIONs coated with different saccharides could show variations drastically in cell responses and viability with minor changes in coatings.

It is assumed that SPIONs could cause at least four primary sources of oxidative stress. According to several studies, it seems that there is a direct impact of SPIONs on ROS damage. Alekseenko *et al*. [240] examined the effects of uncoated SPIONs on neuronal cells. Theil *et al.* [241] investigated the role of ferritin (natural iron storage protein) which seems to have a pivotal role for the direct generation of ROS in rat synaptosomes. Further, Li *et al.* [242] stated that the redox active surface of SPIONs could seriously affect electron flow and alter mitochondrial functionality. Keeping this in mind it can be supposed that the use of active reductase enzymes for toxicological tests within the mitochondria of living cells leads to severe hazards.

Other recognisable targets for SPIONs toxicity seem to be the plasma membrane and proteins [243, 244] where nicotinamideadenine dinucleotide phosphate oxidase and its analogues are considered targets for SPIONs induced redox reactions. Take-up of SPIONs by phagocytic cells both *in vitro* and *in vivo* environments is extensively studied in [245-247].

Inflammation induction has been investigated for both coated and uncoated SPIONs. Siglienti *et al.* [248] found that loading macrophages with SPIONs (uncoated) lead to increased interleukon-10 production and inhibition of tumour necrosis factor α which could be an indication for immunomodulatory function. In the report of Hsiao *et al*. [249] about the response of SPIONs ferucarbotran loading on macrophages and come to the conclusion specific levels of nanoparticles cause secretion of tumour necrosis factor α and production of nitric oxide. It was also found [250] that significant inflammation response is observed when coated anionic SPIONs are used for labelling of human gingival fibroblasts (increase secretion of metalloproteases). Radu *et al*. [251] investigated the impacts of SPIONs on lipid peroxidation and antioxidative systems in lung fibroblast cells showing that an increased lipid peroxidation is observed. In the study of Choi *et al.* [252] *in vitro* cytotoxicity of iron oxide Fe_3O_4 and manganese oxide MnO was investigated by various toxicity assays where different factors were taken into account (the concentration of nanoparticles, incubation time, and different human cell lines). The toxicity has been checked by changes in pH and composition in cells and the tendency of SPIONs to adsorb proteins, vitamins, amino acids, and ions. As discussed by the authors some of the results obtained show that the toxicity assays used for assessing SPIONs are not entirely adapted for this goal and could lead to wrong interpretation.

5.2. *In vivo* toxicity assessment

Natarajan *et al*. [253] employed magnetic nanoparticles with diameters of 20, 30, and 100 nm and evaluated their application for alternating magnetic field therapy and their in vivo performance depending on their size. The results showed that tumour targeting and heating capacity depended on the size of the nanoparticles.

SPIONs are often determined as biocompatible when no significant toxic effects *in vivo* are shown. Jain *et al.* [254] report that *in vivo* administration of SPIONs did not lead to an adverse effect on liver function. It is worth to mention that the correct prediction of the biological fate of SPIONs is strongly dependent on the composition and amounts of associated proteins at the surface of the nanomaterial. For instance, oleic acid/pluronic-coated SPIONs (i.e., 55% of the intravenously injected dose) were found to accumulate in the liver of rats; however, elimination of dextran-coated SPIONs,

via urine and feces, was around 25% of injected dosage in the same animal model [255]. The differences in these studies are probably related to the protein corona composition of the nanoparticles.

The physicochemical parameters of the nanoparticles are usually accepted as an important factor for cell uptake. Mahmoudi *et al.* [256] indicate that cell type is also an important feature for cellular uptake, intracellular fate, and toxic response of the nanoparticles. As shown in this study SPIONs having a different surface chemical composition (uncoated and cyanoethyltrimethoxysilane - and aminopropyltriethoxysilane-coated) revealed toxic impacts on human brain cells at iron concentrations above 2.25 mM, whereas the same concentration of NPs was acceptable for human kidney cells.

Hanini *et al.* [257] tested SPIONs *in vivo* and could confirm that SPIONs induced toxicity in the liver, kidneys, and lungs; however, the brain and heart organs remained unaffected. It is in good agreement with earlier statements that negatively charged SPIONs do not cause serious changes in the actin skeleton of heart cells but could disrupt the actin skeleton in kidney and brain. In the study of Chertok *et al.* [258] on the possibility of applying SPIONs as drug delivery remedy in the magnetic targeting of brain tumours is shown that accumulation of SPIONs in gliosarcomas in rats could be enhanced by suitable concentration of nanoparticles and optimal parameters of the magnetic field without any toxicity effects.

6. Computational Study of SPIONs

From an experimental point of view, the molecular design of SPIONs for biomedical applications is a great challenge. At the nanolevel, the efficiency of molecular design of SPIONs depends on the fundamental understanding of structural concepts and interfacial interactions in the nanoparticle-coating complex. For example, it is essential to know what nanoparticle composition (iron oxide phase and an organic/inorganic coating) is suitable for a given biomedical application and why? Moreover, under an applied magnetic field, superparamagnetic particles can self-assembly in structures, such as chains and bundles. For stimuli-responsive materials and magnetophoresis applications, such self-assembly is the desired effect. On the other hand, for some biomedical applications, the self-assembly should be avoided because it by reducing the biocompatibility, by causing ageing or time dependency in properties [259]. Therefore, at the microscopic level, the efficiency of SPIONs design is determined by the state-of-the-art in methods for self-assembly, i.e. by the knowledge how to control the nanoparticle-nanoparticle and nanoparticle-environment interactions. However, the molecular design of SPIONs is still largely empirical, and the system complexity limits

their experimental multi-scale characterization in bio environment. This hampers the possibility to guide the synthesis and to tune the performance of SPIONs materials for biomedical applications. Therefore, computer simulations and modelling methods play a crucial role in the improvement of molecular designs strategies in SPIONs with biomedical applications.

In this section, we will give a brief overview of the application of the computational methods for SPIONs with attractive biomedical properties. The overview is focused mainly on three widely used and very popular types of computer simulations for SPIONs - molecular dynamics (MD), Monte Carlo (MC) and density functional theory (DFT). The time evolution of a system composed of interacting particles - atoms, molecules or their clusters can be theoretically predicted by using MD method [260, 261]. In this simulation technique, the potential energy of the particle-particle interactions is described by using interatomic potentials or molecular mechanics force fields, the trajectories of the particles are obtained by numerical solution of Newton's equations of motion, and means of statistical mechanics derives the macroscopic properties of the system. Monte Carlo method relies on equilibrium statistical mechanics [262]. It uses random numbers to generate an ensemble of representative configurations of the system, from which thermodynamic properties can be calculated. Monte Carlo simulations are free of solving Newton's equations of motion and do not provide information about the time evolution. Similar to the case of MD, in MC the potential energy of the particle-particle interactions is described by using interatomic potentials or molecular mechanics force fields. Density functional theory is a quantum-mechanical method and is based on the solution of the Schrödinger equation. Therefore, DFT approach is applied to investigate the electronic structure and properties of atoms, molecules and solids – information that is crucial for the SPIONs performance but cannot be obtained by MD and MC simulations. By using DFT method one can model and predict molecular structures, IR and UV-vis spectra, ionisation potential and electron affinity, as well as conducting optical and magnetic properties.

MD simulations have been used in the context of SPIONs to study interfacial interactions of coated nanoparticles, adsorption properties of molecules, proteins and gold nanoparticles. Also, the effect of the magnetic field to permeabilization to cell membranes is also explored by MD calculations.

Qiang *et al.* [263] applied atomistic molecular dynamics simulations and COMPASS force field (Condensed-phase Optimized Molecular Potentials for Atomistic Simulation Studies) to investigate the interfacial interactions in a Fe_3O_4 surface coated with chitosan. They calculated the interaction energy, radial distribution function and concentration profiles for chitosan adsorbed on different Fe_3O_4 crystallographic planes. The result indicated that the interaction of chitosan with Fe_3O_4 (1 1 1) surface is stronger than that with (1 1 0) and (0 0 1) surfaces. The higher probability explains this of formation

of hydrogen bonds between the amino groups of chitosan and the oxygen atoms from the (1 1 1) surface. In another theoretical study by Qiang *et al.* [264] the same computational strategy was used to reveal the interfacial interaction between Fe_3O_4 (1 1 1) crystallographic plane and different biocompatible polymers. In particular, the authors explored coatings based on polysaccharides (chitosan and dextran) and polyesters (polyethylene glycol, polyethylenemine, polylactic acid, and poly(lactic-co-glycolic) acid). The MD study reveals stronger interfacial interactions in the case of polysaccharides than in the case of polyesters. The stronger interfacial interactions with polysaccharides are suggested to originate from the presence of hydrogen donor groups (such as hydroxyl and amino groups) that ensure hydrogen bond formation with the oxygen atoms from the Fe_3O_4 (1 1 1) surface.

Using molecular dynamics simulations and charge consistent-valence force field Harris *et al.* [265] investigated the adsorption of sebacic acid and 1,10-decanediol on the surfaces of Fe_3O_4 nanoparticle ($d \leq 2.6$ nm). The calculations predicted stronger interfacial interactions in the case of 1,10-decanediol coating and showed that only this surfactant inhibits the oxidation of the Fe_3O_4 nanoparticle for the given size range. The theoretical findings are additionally confirmed by experimentally obtained transmission electron micrographs and X-ray diffraction spectra. Two years later, Harris *et al.* [266] reported theoretical results on the adsorption of oleic acid and oleylamine acid on Fe_3O_4 spherical nanoparticles (d=2.6 nm) obtained by the same computational procedure. The organic coatings by different oleic acid/oleylamine acid ratios, are modelled, as well as by changing the degree of protonation of the oleic acid. The authors concluded that the combination of two surfactants is crucial for the synthesis of Fe_3O_4 nanoparticles because the proton accepting properties of the oleylamine acid regulate the electrostatic pressure, which prevents for oleic acid desorption caused by an excess of free protons. Such regulation of the electrostatic pressure and stabilisation is possible only at an ideal ratio of oleic acid/oleylamine acid ratios, which ensures a perfect fit between the surface charge of the nanoparticle, free proton concentration in the dispersion medium, and zeta potential. The computational results are corroborated by transmission electron microscopy (TEM), FTIR, and pH measurements.

Yue *et al.* [267] applied the molecular dynamics method and COMPASS force field. The authors investigated the deposition of gold nanoparticles on the Fe_3O_4 nanoparticles coated with an intermediate layer. The SPIONs core is modelled by Fe_3O_4 (1 1 1) surface, and the intermediate layer is composed by oleylamine, oleic acid, polyethylimine, polymethylacrylic acid, 3-aminopropyl triethylsilane, or tetraethylorthosilicate. Their results indicated that the intermediate layer introduces

new functional groups such as carboxylates, amines, or thiols, which ensure better adsorption of gold nanoparticles on the Fe_3O_4 (1 1 1) surface. Moreover, they showed that the strength of linkage between the Fe_3O_4 (1 1 1) surface and the gold nanoparticles depends on the type of the functional groups present in the intermediate layer. The intermediate coatings with amino groups (oleylamine, polyethylimine and 3-aminopropyl triethylsilane) form a strongly bonded "primary layer" on the Fe_3O_4 (1 1 1) surface but loosely packed "secondary layer", which is critical for the subsequent golden nanoparticles deposition. The authors also considered the interaction of cysteine with Au/polyethylimine/Fe_3O_4 nanocomposites and showed that the amino acid relatively strong absorption, which can be useful for functional exploration in biomedical applications, Fig. 9.

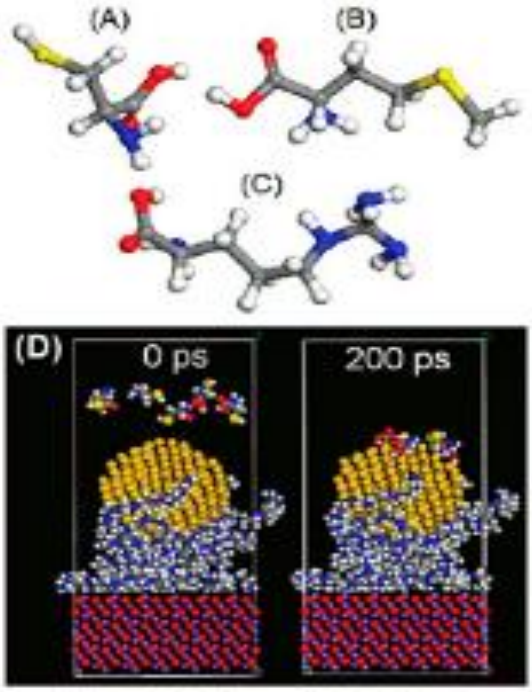

Fig. 9. Molecular structure of (A) cysteine, (B) methinone, and (C) arginine and (D) snapshots of the Au/PEI/Fe_3O_4 nanocomposite with the addition of cysteine at simulation time of 0 and 200 ps - Reprinted with permission from Yue J, Jiang X, Yu A, J. Phys. Chem. B, 2011, 115: 11693 [267]. Copyright [Copyright © 2011 American Chemical Society].

Yu *et al.* [268] employed molecular dynamics simulations to reveal the adsorption of proteins, in particular, bovine serum albumin, on SPIONs. The bovine serum albumin proteins were modelled with an atomistic resolution by using the CHARMM27 force field, and the NPswere simulated as clusters of Lennard-Jones spheres. The solvent effects were also included by employing a generalised

Born implicit solvent model. The authors computed the maximum theoretical number of albumin molecules adsorbed onto the NPs (*d*=6 nm) by simulating SPIONs complexes with 1, 2, 4, 8, 10, and 12 protein molecules. The computational results suggest monolayer of 10 bovine serum albumin molecules on one NP, which is also confirmed by experimental TEM and UV-vis measurements. The MD simulations also revealed three different stages in the adsorption process of bovine serum albumin proteins: (1) the protein migrates from the bulk solution in order to get in touch with the NP surface, (2) the protein spreads out on the NP surface in a view to increase the contact region with the core (3) the protein relaxes to a more compact configuration The findings suggested that due to its protein-resistant surface the bovine serum albumin-SPIONs complex can be used as an efficient carrier for targeted drug delivery *in vivo*.

Recently, Pedram *et al.* [269] explored the magnetic field effect to deliver SPIONs through the blood-brain barrier using molecular dynamics simulations and CHARMM27 force field. The solvent effects were also taken into account by using the TIP3P method for water. The endothelial cell membrane of the blood-brain barrier is modelled as a lipid bilayer of palmitoyl oleyl phosphatidyl choline (POPC). The SPIONs are simulated as are spherical shaped particles with 2 nm size with a gold coating (2 Å). The calculations reveal that by applying a magnetic force in the range of pN, the SPIONs open a gap in the membrane and cross it, Fig. 10. Moreover, this process is reversible and totally non-invasive. Afterwards, the SPIONs can move through the cells with a much lower magnetic force. The results show that the maximum magnetic force depends on the nanoparticle size and that the crossing time can be controlled by variation of the magnetic pattern and magnetic field strength.

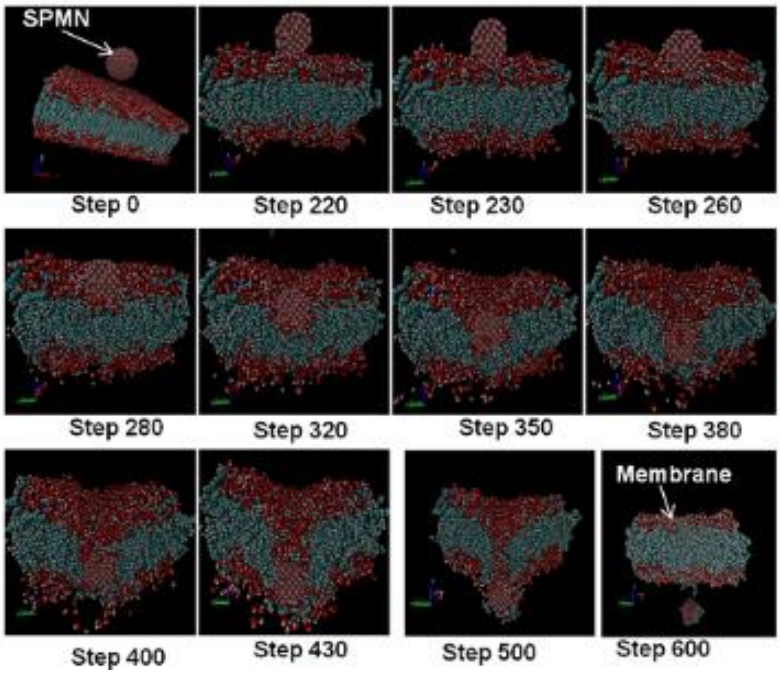

Fig. 10. Several Steps of Crossing through the blood-brain barrier (BBB) These steps come from simulation, and the main goal is to show how the membrane is opened and how it can rehabilitate itself upon the completion of the crossing. Reprinted with permission from Pedram M Z, Shamloo A, Alasty A, Ghafar-Zadeh E, Biosensors 2016, 6: *25* [269].

The Monte Carlo method is a stochastic method and has been employed to generate a statistical or probabilistic model for understanding particular systems. The MC calculations were performed to confirm the experimentally observed behaviour of Fe_3O_4 nanoparticles and SPIONs. MC calculations were conducted to compute: adsorption of molecules as water and surfactant molecules, the stability of dispersions, and to simulate the T_2 relaxation in magnetic resonance experiments.

Tombácz *et al.* [270] investigated the adsorption of water vapour on the surface of Fe_3O_4 nanoparticles by using grand canonical Monte Carlo method. The authors applied Universal force field (UFF) and TIP4P model of the water. The NP surface is simulated as a (001) and (011) surface of the magnetite crystal. The theoretically predicted adsorption isotherm reproduces very well the measured ones. The calculations show the adsorbed water is organised in a layered structure, which occurs by simultaneous formation of several molecular layers. The simulations also suggest that the adsorption mechanism is similar to nucleation, i.e. new water molecules are attracted to the surface regions that already accommodate a large amount of water.

Experimental results of Kumar *et al.* [271] show a different state of dispersion for Fe_3O_4 nanoparticles in an aqueous medium as a function of the nanoparticle coating. Namely, aggregates formation for Fe_3O_4 nanoparticles coated with citric acid and an individual isolated state for Fe_3O_4 nanoparticles coated. MC calculations were performed to confirm the experimentally observed behaviour of the aqueous dispersions. To get further insight on the stability of the dispersions, the authors simulated the effect of four variables: particle volume percentage, particle diameter, shell thickness, and grafting density. Based on the theoretical predictions, the authors were able to recommend a possible range of values for these four variables, which can be directly applied experimentally to obtain a stable aqueous dispersion of isolated particles.

Matsumoto *et al.* [272] used MC method to simulate the T_2 relaxation induced by clusters of SPIONs in magnetic resonance experiments. The authors calculated the T_2 relaxation as a function of different geometric characteristics of the nanoparticle clusters: particle size, the number of particles per cluster, interparticle distance, compact or linear cluster shapes. The simulations reveal that for small particles, the cluster shape and cluster density significantly affect the T_2 relaxation, while the for large particles the T_2 relaxation become dependent on the cluster geometry only when the interparticle

distances exceeded ten times the particle diameter. These results suggest that the performance of the aggregation-based sensors can be controlled by optimising the SPIONs size and coating thickness and that the changes in the magnetic resonance imaging contrast could be obtained by tuning the geometric parameters of the individual clusters.

Martinez-Boubeta *et al.* [273] performed MC simulations on SPIONs to describe their magnetic hyperthermia performance theoretically. The MC calculations were carried out by using atomistic and macrospin approximation approaches. The atomistic MC calculations corroborate experimental measurements and show larger anisotropy in the case of the cubic than regarding spherical nanoparticles. Also, the authors reported a qualitative relationship between the heat power and the interparticle interactions. Namely, they demonstrated that the assembling of the cubic nanoparticles in elongated chains represents a promising way to increase the hyperthermia performance.

In their theoretical work, Russier *et al.* [274] reported MC simulations on the mean size and polydispersity effects in densely packed iron oxide magnetic nanoparticles assemblies. The nanoparticles are modelled as uniformly magnetised spheres coated with the insulating organic layer. The results demonstrate that the linear magnetic susceptibility as a function of the median diameter may present a plateau. This was shown to lead to a quasi- independence of the magnetisation on the median diameter at low external fields and high concentration. The magnetocrystalline anisotropy is then proved to play a role for larger values of the field when the particles remain in the superparamagnetic regime in agreement.

Using three-dimensional MC simulations and electron magnetic resonance measurements, Castro *et al.* [275] explored a fluid composed of Fe_3O_4 nanoparticles coated with dodecanoic acid molecules and dispersed in hydrocarbons. The results reveal that the grafting (surface density of surfactant molecules) of isolated particles increases with the particle concentration, while the grafting of bonded nanoparticles shows a more complicated behaviour. The simulations demonstrate that the adsorbed molecules have a tendency to dissociate when the surfactant layers of two nanoparticles get in contact. On the other hand, the repulsion between the apolar solvent and the polar heads dissociated molecules increases the possibility for re-adsorption of the surfactants on available adsorption sites. The results suggest that the ratio between the grafting (steric repulsion) and Hamaker constant (van der Waals attraction) determines the degree of nanoparticle agglomeration.

Many DFT studies have emphasised on the structural, electronic, catalytic, and magnetic properties of Fe_2O_3 and SPIONs. Methods developed in the framework of DFT are currently the most popular and effective approaches used in solid state physics, quantum chemistry and nanotechnology.

DFT investigation of the stability of SPIONs coatings in the physiological environment was reported by Aschauer *et al.* [276]. The DFT calculations were performed in vacuo with the PBE functional, taking into account van der Waals correction. The SPIONs were modelled by the (1 1 0) surface of Fe_3O_4 and coating molecules were represented by water, polyvinyl alcohol, polyethylene glycol, monomer and dimer of glycine as a prototype short peptide. The theoretical results show that the adsorption energy decreases in the following order: polyvinyl alcohol > water > polyethylene glycol ~ glycine. This proposes the stability of the polyvinyl alcohol coatings in the presence of water and polypeptides. The higher adsorption strength of polyvinyl alcohol was explained by the presence of OH side-group, which binds significantly stronger to the surface than the oxygen from the polyethylene glycol or the amino group of the peptide bond.

Guénin *et al.* [277] reported a combined DFT and experimental study on the ligand exchange on the surface of SPIONs dispersed in water. The authors compared two strong chelating agents, containing catechol and bisphosphonate moieties. The DFT calculations were performed with the exchange-correlation functional of Staroverov, Scuseria, Tao and Perdew functional (TPSSh), and they served to elucidate the interactions between catechol/bisphosphonate groups and the nanoparticle surface. The calculated spectra show good agreement with the FTIR measurements and confirm that the adsorption of ligands is realised through their chelating groups. The experimental results demonstrate that catechol and bisphosphonate molecules can be exchanged and that the ligand exchange increases by using a large excess of bisphosphonate and sonication.

Fouineau *et al.* [278] demonstrated that the DFT simulations with the Perdew, Burke, and Ernzerhof (PBE) functional could be used to elucidate the electronic transfer and the binding mode between coating ligands of biological interest and the SPIONs surface. In particular, the authors investigated γ-Fe_2O_3 nanoparticles functionalized with dopamine; the results reveal that dopamine binds preferentially to octahedral sites and that the linking bond is with covalent nature. Experimental data corroborate the results, and the agreement proves that the DFT simulations can serve as an appropriate supplemental approach to interpreting ^{57}Fe Mössbauer spectra of SPIONs.

By using DFT method, de Leeuw *et al.* [279] investigated the hydration behaviour of three iron (hydro)oxide minerals, including hematite. The results suggest that the interaction with water molecules is done mainly between the oxygen and the surface iron ions from the hematite surface, followed by hydrogen-bonding to surface oxygen ions. The calculations show relatively larger hydration energies for hematite and dissociative adsorption of water molecules.

Faraudo and co-workers [280] explored and analysed magnetophoretic separation of superparamagnetic particles under well-controlled magnetophoretic conditions. The authors obtained a simple analytical solution for the process of noncooperative magnetophoresis by which its kinetics can be predicted based on particle characterization data, such as size and magnetisation. In another paper by Faraudo *et al.* [281] devoted to the theoretical aspects of cooperative magnetophoresis of superparamagnetic colloids, the authors analysed the physicochemical conditions at which reversible aggregation occurs, the timescale of aggregate formation and their aggregates shape. In the case of colloids stabilised electrostatically, they found that the interaction potential between two superparamagnetic particles is such that allows the reversible formation of aggregates. Also, the authors reported that the particle aggregation is a fast process and the preferred aggregation is lateral over the tip-to-tip aggregation for long chains. These findings are in agreement with experimental observations. An excellent review on computational methods for qualitative prediction of self-assembly processes of SPIONs can find in the very recent publication of Faraudo *et al.* [259].

The above-presented investigations clearly illustrate the predictive power of the theoretical modelling for efficient design of SPIONs structures, aggregation behaviour and properties. To go deeper in the understanding of the intimate structural, chemical, and physical properties of functionalized SPIONs, we want to focus the attention of the reader to the role and impact of the computational methods rely on multiscaling approach.

Conclusions:

The assessment of the role of SPIONs as a versatile platform for medical development requires more in-depth insight knowledge and constant study of relationships between nanoparticles size and size distribution, shape, surface coating, magnetic properties and their biological application. The focus of the review is on recent progress in this field, and the diverse utilities of SPIONs for diagnostics, therapeutics and theranostics are outlined. A general discussion on the *in vitro* and *in vivo* toxicities of SPIONs has been provided while there are still some issues that need to be explicitly addressed during the engineering of SPIONs for clinical use. It is crucial to understand the potential risks associated with exposure to SPIONs and the physiological effects produced by the surface coatings utilised for functionality considering the broad ~~a~~pplications of SPIONs. The review also has highlighted the ability of computational models as a valuable tool for better understanding of the system to obtain proper materials with the desired behaviour and properties. In this respect, theoretical methods, in the form of analytical equations or computational methods could be very helpful to shed light on the topic.Through

the persistent efforts by multidisciplinary and multilevel approaches, there is a great potential for further breakthrough developments in SPIONs designs for nanomedicine application.

Acknowledgements

This work was financed by the European Union H2020 Programme (H2020) under grant agreement 692146-H2020-eu.4.b "Materials Networking" (MN, BD, GT, SM, VS), COST Action MP1306 (MN, GT), Bulgarian Science Fund under Grant agreement DCOST-01/18 (MN, BD), Bulgarian Science Fund under Grant agreement DCOST-01/18 (GT), and the grant 2014SGR107 (SM).

REFERENCES

[1]. Erb RM, Yellen BB. In: Liu JP, Fullerton E, Gutfleisch O, Sellmyer DJ (editors), Nanoscale Magnetic Materials and Applications. Springer; 2009. Chapter 19.

[2]. Hofmann-Amtenbrink M, von Rechenberg B, Hofmann H. In: Tan MC (editor), Nanostructured Materials for Biomedical Applications. Transworld Research Network, Kearala, India; 2009. Chapter 5.

[3]. Gilchrist R, Medal R, Shorey WD, Hanselman RC, Parrott JC, Taylor CB, Ann Surg, 1957; 146: 596.

[4]. Saini S, Stark D, Hahn P, Wittenbemg J, Brady T, Fermucci J, Radiology, 1987; 162: 211.

[5]. Weissleder R, Hahn PF, Stark DD, Elizondo G, Saini S, Todd LE, Wittenberg J, Ferrucci JT, Radiology, 1988; 169: 399.

[6]. Weissleder R, Elizondo C, Wittenberg J, Lee AS, Josephson L, Brady TJ, Radiology, 1990; 175: 494.

[7]. Jordan A, R Scholz, K Maier-Hauff, Johannsen M, Wust P, Nadobny J, Schirra H, Schmidt H, Deger S, Loening S, Lanksch W, J Magn Magn Mater, 2001; 225: 118.

[8]. Horák D, Polymer, 2005; 46: 1245.

[9]. Neuberger T, Schöpf B, Hofmann H, Hofmann M, von Rechenberg B, J Magn Magn Mater, 2005; 293: 483.

[10]. Bárcena C, Sra AK, Gao J. In: Liu JP, Fullerton E, Gutfleisch O, Sellmyer DJ (editors), Nanoscale Magnetic Materials and Applications. Springer; 2009. Chapter 20.

[11]. Dutz S, IEEE Trans Magn, 2016; 52: 1.

[12]. Krishnan KM, IEEE Trans Magn, 2010; 46: 2523.

[13]. Colombo M, Carregal-Romero S, Casula MF, Gutiérrez L, Morales MP, Böhm IB, Heverhagen JT, Prosperi D, Parak WJ, Chem Soc Rev, 2012; 41: 4306.

[14]. Kuncser V, Palade P, Kuncser A, Greculeasa S, Schinteie G. In: Kuncser V, Miu L (editorss), Size Effects in Nanostructures: Basics and Applications. Springer; 2014. Chapter 7.

[15]. Kandasamy G, Maity D, Int J Pharm, 2015; 496: 191.

[16]. Tombácz E, Turcu R, Socoliuc V, Vékás L, Biochem Biophys Res Commun, 2015; 468: 442.

[17]. Nowak J, Wiekhorst F, Trahms L, Odenbach S, J Phys Condens Matter, 2014; 26: 176004.

[18]. Nowak J, Nowak C, Odenbach S, Appl Rheol, 2015; 25: 53250.

[19]. Gupta AK, Gupta M, Biomater, 2005; 26: 3995.

[20]. Tartaj P, Morales MP, Veintemillas-Verdaguer S, Gonzalez-Carreno T, Serna CJ. In: Buschow KHJ. (editor), Handbook of Magnetic Materials, Vol. 16. Elsevier; 2006, Chapter 5.

[21]. Laurent S, Forge D, Port M, Roch A, Robic C, Vander Elst L, Muller RN, Chem Rev, 2008; 108: 2064.

[22]. Veiseh O, Gunn JW, Zhang M, Adv Drug Deliv Rev, 2010; 62: 284.

[23]. Oh JK, Park JM, Prog Polym Sci, 2011; 36: 168.

[24]. Reddy LH, Arias JL, Nicolas J, Couvreur P, Chem Rev, 2012; 112: 5818.

[25]. Lam T, Pouliot P, Avti PK, Lesage F, Kakkar AK, Adv Colloid Interface Sci, 2013, 199–200: 95.

[26]. Turcheniuk K, Tarasevych AV, Kukhar VP, Boukherroub R, Szunerits S, Nanoscale, 2013; 5: 10729.

[27]. Wu W, Wu Z, Yu T, Jiang C, Kim W S, Sci Technol Adv Mater, 2015; 16: 023501

[28]. Ling D, Lee N, Hyeon T, Acc Chem Res, 2015; 48: 1276.

[29]. Gutiérrez L, Costo R, Grüttner C, Westphal F, Gehrke N, Heinke D, Fornara A, Pankhurst QA,.Johansson C, Veintemillas-Verdaguer S, Morales MP, Dalt Trans, 2015; 44: 2943.

[30]. Lartigue L, Hugounenq P, Alloyeau D, Clarke SP, Lévy M, Bacri JC, Bazzi R, Brougham DF, Wilhelm C, Gazeau F, ACS Nano, 2012; 6: 10935.

[31]. Gavilán H, Posth O, Bogart LK, Steinhoff U, Gutiérrez L, Puerto Morales M, Acta Materialia, 2017; 125: 416.

[32]. Bhavani P, Rajababu CH, Arif MD, Reddy IVS, Reddy NR, J Magn Magn Mater, 2017; 426: 459.

[33]. Bonvin D, Hofmann H, Ebersold MJM, Nanopart Res, 2016; 18: 376.

[34]. Beg MS, Mohapatra J, Pradhan L, Patkar D, Bahadur D, J Magn Magn Mater, 2017; 428: 340.

[35]. Sun Z, Cheng K, Wu F, Liu H, Ma X, Su X, Liu Y, Xia L, Cheng Z, Nanoscale, 2016; 8: 19644

[36]. Wan J, Yuan R, Zhang C, Wu N, Yan F, Yu S, Chen K, J Phys Chem C, 2016; 120: 23799.

[37]. Thorat ND, Lemine OM, Bohara RA, Omri K, El Mir L, Tofail SAM, Phys Chem Chem Phys, 2016; 18: 21331.

[38]. Richard S, Eder V, Caputo G, Journé C, Ou P, Bolley J, Louedec L, Guenin E, Motte L, Pinna N, Lalatonne Y, Nanomedicine, 2016; 11: 2769.

[39]. Antonelli A, Sfara C, Weber O, Pison U, Manuali E, Magnani M, Nanomedicine, 2016; 11:2781

[40]. Etheridge ML, Campbell SA, Erdman AG, Haynes CL, Wolf SM, McCullough J, Nanomed Nanotechnol Biol Med, 2013; 9: 1.

[41]. Bregoli L, Movia D, Gavigan-Imedio JD, Lysaght J, Reynolds J, Prina-Mello A, Nanomed Nanotechnol Biol Med, 2016; 12: 81.

[42]. Reflection paper on the data requirements for intravenous iron-based nano-colloidal products developed with reference to an innovator medicinal product, EMA/CHMP/SWP/620008/2012, European Medicines Association, 2015.

[43]. Wang YXJ, World J Gastroenterol, 2015; 21: 13400.

[44]. Wáng YXJ, Idée J-M, Quant Imaging Med Surg, 2017; 7: 88.

[45]. Rinck P, J Magn Reson Imaging, 2001; 13: 485.

[46]. Figuerola A, Di Corato R, Manna L, Pellegrino T., Pharmacol Res, 2010; 62: 126.

[47]. Mahmoudi M, Sahraian MA, Shokrgozar MA, Laurent S, ACS Chem Neurosci, 2011; 2: 118.

[48]. Sharifi S, Seyednejad H, Laurent S, Atyabi F, Saei A, Mahmoudi M, Contrast Media Mol Imaging, 2015; 10: 329

[49]. Na HB, Song I C, Hyeon TW, Agents Adv Mater, 2009; 21: 2133.

[50]. Thomsen HS, Radiol Clin North Am, 2009; 47: 827.

[51]. Mendichovszky IA, Marks SD, Simcock CM, Olsen ØE, Pediatr Radiol, 2008; 38: 489.

[52]. Khawaja AZ, Cassidy DB, Al Shakarchi J, McGrogan DG, Inston NG, Jones RG, Insights Imaging, 2015; 6: 553.

[53]. Pierre VC, Allen MJ, Caravan P, J Biol Inorg Chem, 2014; 19: 127.

[54]. Linderoth S, Hendriksen PV, Bodker F, Wells S, Davies K, Charles SW, Morup SJ, Appl Phys, 1994; 75: 6583.

[55]. Morales MP, Veintemillas-Verdaguer S, Montero MI, Serna CJ, Roig A, Casas L, Martinez B, Sandiumenge F, Chem Mater, 1999 ; 11: 3058.

[56]. Kim BH, Lee N, Kim H, An K, Park, YI, Choi Y, Shin K, Lee Y, Kwon SG, Na HB, Park JG, Ahn, TY, Kim YW, Moon WK, Choi SH, Hyeon T, J Am Chem Soc, 2011; 133: 12624.

[57]. Taboada E, Rodríguez E, Roig A, Oró J, Roch A, Muller RN, Langmuir, 2007; 23: 4583.

[58]. Tromsdorf UI, Bruns OT, Salmen SC, Beisiegel U, Weller H, Nano Lett, 2009; 9: 4434.

[59]. Zeng L, Ren W, Zheng J, Cui P, Wu A, Phys. Chem. Chem. Phys, 2012; 14: 2631.

[60]. Sandiford L, Phinikaridou A, Protti A, Meszaros LK, Cui X, Yan Y, Frodsham G, Williamson PA, Gaddum N, Botnar RM, Blower PJ, Green M A, de Rosales RTM, ACS Nano, 2013; 7: 500.

[61]. Xiao W, Lin J, Li M, Y Ma, Y Chen, C Zhang, Li D, Gu H, Contrast Media Mol Imaging, 2012; 7: 320.

[62]. Schnorr J, Wagner S, Abramjuk C, Wojner I, Schink T, Kroencke TJ, Schellenberger E, Hamm B, Pilgrimm H, Taupitz M, Invest. Radiol, 2004; 39: 546.

[63]. Taupitz M, Wagner S, Schnorr J, Kravec I, Pilgrimm H, Bergmann-Fritsch H, Hamm B, Invest Radiol, 2004; 39: 394.

[64]. Liu CL, Peng YK, Chou SW, Tseng WH, Tseng YJ, Chen HC. Hsiao JK, Chou PT, Small, 2014; 10: 3962.

[65]. Shen Z., Wu A., Chen X. (2016). Iron Oxide Nanoparticle Based Contrast Agents for Magnetic Resonance Imaging. Molecular Pharmaceutics, http://pubs.acs.org/doi/abs/10.1021/acs.molpharmaceut.6b00839

[66]. Borase T, Ninjbadgar T, Kapetanakis A, Roche S, O'Connor R, Kerskens C, Heise A, Brougham DF, Angew Chem Int Ed, 2013; 52: 3164.

[67]. Ling D, Park W, Park SJ, Lu Y, Kim KS, Hackett MJ, Kim BH, Yim H, Jeon YS, Na K, Hyeon T, J Am Chem Soc, 2014; 136: 5647.

[68]. Zhang H., Li L., Liu X.L., Jiao J., Ng C.-T., Yi J.B., Luo Y.E., Bay B.-H., Zhao L.Y., Peng M.L, Gu N., Fan H.M. (2017). Ultrasmall Ferrite Nanoparticles Synthesized via Dynamic Simultaneous Thermal Decomposition for High-Performance and Multifunctional T_1 Magnetic Resonance Imaging Contrast Agent. ACS Nano, http://pubs.acs.org/doi/abs/10.1021/acsnano.6b07684

[69]. Chen R, Ling D, Zhao L, Wang S, Liu Y, Bai R, Baik S, Zhao Y, Chen C, Hyeon T, ACS Nano, 2015; 9: 12425.

[70]. Lee N, Yoo D, Ling D, Cho M H, Hyeon T, Cheon J, Chem Rev, 2015; 115: 10637.

[71]. Zanganeh S, Jim Q, Jafari T, Khakpash N, Erfanzadeh M, Spitler R, J Clin Med Imaging, 2016; 2: 100.

[72]. Yoo D, Lee JH, Shin TH, Cheon J, Acc Chem Res, 2011; 44: 863.

[73]. Koenig SH, Kellar KE, Magn Reson Med, 1995; 34: 227.

[74]. Roch A, Muller RN, Gillis P, J Chem Phys, 1999; 110: 5403.

[75]. Vuong QL, Berret JF, Fresnais J, Gossuin Y, Sandre O, Adv Healthcare Mater, 2012; 1: 502.

[76]. Gillis P, Moiny F, Brooks RA, Magn Reson Med, 2002; 47: 257.

[77]. Tong S, Hou S, Zheng Z, Zhou J, Bao G, Nano Lett, 2010; 10: 4607.

[78]. Jun Y, Huh Y-M, Choi J, Lee J, Song H, Kim S, Yoon S, Kim K, Shin J, Suh J, Cheon J, J Am Chem Soc, 2005; 127: 5732.

[79]. Mohapatra J, Mitra A, Tyagi H, Bahadur D, Aslam M, Nanoscale, 2015; 7: 9174.

[80]. Mohapatra J, Mitra A, Aslam M, Bahadur D, IEEE Trans Magn, 2015; 51: 7114261.

[81]. Gillis P; Moiny F; Brooks RA, Magn Reson Med, 2002; 47: 257.

[82]. Brooks R, Magn Reson Med, 2002; 47: 388.

[83]. Gossuin Y, Gillis P, Hocq A, Vuong QL, Roch A, Nanomed Nanobiotechnol, 2009; 1: 299.

[84]. Lee N, Choi Y, Lee Y, Park M, Moon WK, Choi SH, Hyeon T, Nano Lett, 2012; 12: 3127.

[85]. Brooks R, Moiny F, Gillis P, Magn Reson Med, 2001; 45: 1014.

[86]. Lee N, Kim H, Choi SH, Park M, Kim D, Kim H, Proc Natl Acad Sci USA, 2011; 108: 2662.

[87]. Yang Y, Liu X, Lv Y, Herng TS, Xu X, Xia W, Adv Funct Mater, 2015; 25: 812

[88]. Jia CJ, Sun LD, Luo F, Han XD, Heyderman LJ, Yan ZG, J Am Chem Soc, 2008; 130: 16968.

[89]. Zhao Z, Zhou Z, Bao J, Wang Z, Hu J, Chi X, Ni K, Wang R, Chen X, Chen Z, Gao J, Nat Commun, 2013; 4: 2266.

[90]. Mohapatra J, Mitra A, Aslam M, Bahadur D, IEEE Trans Magn, 2015; 51: 7114261.

[91]. Smith CE, Lee J, Seo Y, Clay N, Park J, Shkumatov A, Ernenwein D, Lai MH, Misra S, Sing CE, Andrade B, Zimmerman SC, Kong H, ACS Appl Mater Interfaces, 2017; 9: 1219.

[92]. Chen S, Zhang J, Jiang S, Lin G, Luo B, Yao H, Lin Y, He C, Lin G, Lin Z, Nanosc Res Lett, 2016; 11: 263.

[93]. Saraswathy A, Nazeer SS, Jeevan M, Nimi N, Arumugam S, Harikrishnan VS,Varma PRH, Jayasree RS, Coll Surf B: Biointerfaces, 2014; 117: 216.

[94]. Saraswathy A, Nazeer SS, Nimi N, Arumugam S, Shenoy SJ, Jayasree RS, Carbohydr Polym, 2014; 101: 760.

[95]. Mishra SK, Kumar BS, Khushu S, Tripathi RP, Gangenahalli G, Contrast Media Mol Imaging, 2016; 11: 350.

[96]. Uchiyama MK, Toma SH, Rodrigues SF, Shimada AL, Loiola RA, Cervantes Rodríguez HJ, Oliveira PV, Luz MS, Rabbani SR, Toma HE, Poliselli Farsky SH, Araki K, Int J Nanomedicine, 2015; 10: 4731.

[97]. Xie S, Zhang B, Wang L, Wang J, Li X. Yang G, Gao F, Appl Surf Science, 2015; 326: 32.

[98]. Cano M, de la Cueva-Méndez G, Chem Commun, 2015; 51: 3620.

[99]. Cano M, Núñez-Lozano R, Lumbreras R, González-Rodríguez V, Delgado-García A, Jiménez-Hoyuela JM, de la Cueva-Méndez G, Nanoscale, 2017; 9: 812.

[100]. Margolis L B, Namiot V A, Kljukin L M, Biochim Biophys Acta, 1983; 735: 193.

[101]. Fattahi H, Laurent S , Arsalani N, Elst L, Mullerer R, Nanomedicine, 2011; 6: 529.

[102]. Frascione D, Diwoky C, Almer G, Opriessnig P, Vonach C, Gradauer K, Leitinger G, Mangge H, Stollberger R, Prassl R, Int. J. Nanomed, 2012; 7: 2349.

[103]. Meier S, Pütz G, Massing U, Hagemeyer CE, von Elverfeldt D, Meißner M, Ardipradja K, Barnert S, Peter K, Bode C, Schubert R, von zur Muhlen C, Biomaterials, 2015; 58: 137.

[104]. Faria M, Cruz M, Gonçalves M , Carvalho A, Feio G, Martins M, International Journal of Pharmaceutics, 2013; 446: 183.

[105]. De Cuyper M, Joniau M, Eur Biophys J, 1988; 15: 311.

[106]. Fortin-Ripoche J-P, Martina M S, Gazeau F, Radio, 2006; 239: 415.

[107]. Martínez-González R, Estelrich J, Busquets MA, Int. J. Mol. Sci., 2016; 17: 1209.

[108]. Bárbara M, Martins A F, Corvo M L, Marcelino P, Marinho H S, Feio G, Carvalho A, Nanomed, 2013; 10: 207.

[109]. Shin TH, Choi JS, Yun S, Kim IS, Song HT, Kim Y, Park KI, Cheon J, ACS Nano, 2014; 8: 3393.

[110]. Choi JS, Lee JH, Shin TH, Song HT, Kim EY, Cheon J, J Am Chem Soc, 2010; 132: 11015.

[111]. Chan N, Laprise-Pelletier M, Chevallier P, Bianchi A, Fortin MA, Oh JK, Biomacromolecules, 2014; 15: 2146.

[112]. Zhou Z, Zhao Z, Zhang H, Wang Z, Chen X, Wang R, Chen Z, Gao J, ACS Nano, 2014; 8: 7976.

[113]. Ghobril C, Popa G, Parat A, Billotey C, Taleb J, Bonazza P, Begin-Colin S, Felder-Flesch D, Chem. Commun, 2013; 49: 9158.

[114]. Basly B, Felder-Flesch D, Perriat P, Pourroy G, Bégin-Colin S, Contrast Media Mol Imaging, 2011; 6: 132.

[115]. Basly B, Popa G, Fleutot S, Pichon BP, Garofalo A, Ghobril C, Billotey C, Berniard A, Bonazza P, Martinez H, Felder-Flesch D, Begin-Colin S, Dalton Trans, 2013; 42: 2146.

[116]. Zhou Z, Huang D, Bao J, Chen Q, Liu G, Chen Z, Chen X, Gao J, Adv. Mater. 2012; 24: 6223.

[117]. Yang H, Zhuang Y, Sun Y, Dai A, Shi X, Wu D, Li F, Hu H, Yang S, Biomaterials 2011; 32, 4584.

[118]. Wang Z, Liu J, Li T, Liu J, Wang B, J Mater Chem B, 2014; 2: 4748.

[119]. Cherry SR, Louie Y, Jacobs RE, Proc. IEEE, 2008; 96: 416.

[120]. Jennings LE, Long NJ. Chem Commun, 2009; 24; 3511.

[121]. Louie A, Rev, 2010; 110: 3146.

[122]. Lee DE, Koo H, Sun IC, Ryu JH, Kim K, Kwon IC, Chem Soc Rev, 2012; 41: 2656.

[123]. Rieffel J, Chitgupi U, Lovell JF, Small, 2015; 11: 4445.

[124]. Chen M, Yin M, Prog Polym Sci, 2014; 39: 365.

[125]. P Beard, Interface Focus, 2011; 1: 602.

[126]. Tang T, Garcia J, Louie AY. In Bulte JWM, Modo MMJ (editors), Design and Applications of Nanoparticles in Biomedical Imaging, Springer; 2017. Chapter 10

[127]. Townsend DW, Beyer T, Blodgett TM, Nucl Med, 2003; 33: 193.

[128]. Schlemmer HPW, Pichler B J, Townsend DW, Judenhofer MS, Nahmias C, Heiss WD, Claussen CD, . Int. Soc. Magn. Res. Med., 2007; 18: 989.

[129]. Thomas R, Park IK, Jeong YY, Int J Mol Sci, 2013; 14: 15910.

[130]. Chen D, Dougherty CA, Yang D, Wu H, Hong H, Tomography, 2016; 2: 3.

[131]. Ai F, Ferreira CA, Chen F, Cai W, WIREs Nanomed Nanobiotechnol 2016, 8: 619.

[132]. Same S, Aghanejad A, Akbari Nakhjavani S, Barar J, Omidi Y, Bioimpacts, 2016; 6: 169.

[133]. Bass L, Wang M, Welch M, Anderson C, Bioconjugate Chem, 2000; 11: 527.

[134]. Reilly RM, Chen P, Wang J, Scollard D, Cameron R, Vallis KA, J Nucl Med, 2006; 47: 1023.

[135]. de Rosales RTM, Tavaré R, Glaria A,Varma G, Protti A, Blower PJ, Bioconjug Chem 2011; 22: 455.

[136]. de Rosales RTM, Tavaré R, Paul RL, Jauregui-Osoro M, Protti A, Glaria A, Varma G, Szanda I, Blower P, Agent Angew Chem, 2011; 50: 5509.

[137]. Thorek DL, Ulmert D, Diop NF, Lupu ME, Doran MG, Huang R, Nat Commun, 2014; 5: 3097.

[138]. Chen F, Ellison PA, Lewis CM, Hong H, Zhang Y, Shi S, Hernandez R, Meyerand ME, Barnhart TE, Cai W, Angew Chem, 2013; 52: 13319.

[139]. Chakravarty R, Valdovinos HF, Chen F, Lewis CM, Ellison PA, Luo H, Meyerand ME, Nickles RJ, Cai W, Adv. Mater. 2014; 26: 5119.

[140]. Boros E, Bowen AM, Josephson L, Vasdev N, Holland JP, Chem Sci, 2015; 6, 225.

[141]. Burke BP, Baghdadi N, Kownacka AE, Nigam S, Clemente GS, Al-Yassiry MM, Domarkas J, Lorch M, Pickles M, Gibbs P, Tripier R, Cawthorne C, Archibald SJ, Nanoscale, 2015; 7: 14889.

[142]. Pellico J, Ruiz-Cabello J, Saiz-Alía M, del Rosario G, Caja S, Montoya M, de Manuel LF, Morales MP, Gutiérrez L, Galiana B, Enríquez JA, Herranz F, Contr Media Mol Imaging, 2016; 11: 203.

[143]. Xue S, Zhang C, Yang Y, Zhang L, Cheng D, Zhang J, Shi H, Zhang Y, J Biomed Nanotechnol, 2015; 11: 1027.

[144]. Park JI, Dinesh J, Ross W, Wendy O, Siyon C, Greg JS, Kumacheva E, J Am Chem Soc, 2010; 4: 6579.

[145]. Liu Z, Lammers T, Ehling J, Fokong S, Bornemann J,Kiessling F, Gätjens J, Biomaterials, 2011; 32: 6155.

[146]. Brismar TB, Grishenkov D, Gustafsson B, Härmark J, Barrefelt A, Kothapalli SV, Margheritelli S, Oddo L, Caidahl K, Hebert H, Paradossi G, Biomacromolecules, 2012; 13: 1390.

[147]. He W, Yang F, Wu Y, Wen S, Chen P, Zhang Y, Gu N, Mater Lett, 2012; 68: 64.

[148]. Cheng X, Li H, Chen Y, Luo B, Liu X, Liu W, Xu H, Yang X, PLoS One, 2013; 8: e85003.

[149]. Sciallero C, Balbi L,Paradossi G, Trucco A, R Soc Open Sci, 2016; 3: 160063.

[150]. Teraphongphom N, Eisenbrey J, Naha P, Witschey W, Opasanont B, Jablonowski L, Cormode D, Wheatley M, Langmuir, 2015; *31*: 11858.

[151]. Wang C, Kang T, Yeh K, Biomaterials, 2013; 34: 1852.

[152]. Huang H, Hu S, Hung S, Chiang C, Liu H, Chiou T, Lai H, Chen Y, Chen S, J Control Release, 2013; 172: 118.

[153]. Yang P, Luo X, Wang S, Wang F, Tang C, Wang C, Colloids and Surfaces B: Biointerfaces, 2017; 151: 333.

[154]. Malinge J, Géraudie B, Savel P, Nataf V, Prignon A, Provost C, Zhang Y, Ou P, Kerrou K, Talbot JN, Siaugue JM, Sollogoub M, Menager C, Mol Pharm, 2017; 14: 406.

[155]. Zhu J, F. Yan F, Guo Z, Marchant R, J. Colloid Interface Sci, 2005; 289: 542.

[156]. Wilson KE, Valluru KS, Willmann JK. In: Bulte JWM, Modo MMJ (editors), Design and Applications of Nanoparticles in Biomedical Imaging, Springer; 2017. Chapter 15.

[157]. Zhou M, Li L, Yao J, Bouchard RR, Wang LV, Li C. In: Bulte JWM, Modo MMJ (editors), Design and Applications of Nanoparticles in Biomedical Imaging, Springer; 2017. Chapter 16.

[158]. Xu C, Shi S, Feng L, Chen F, Graves SA, Ehlerding EB, Goel S, Sun H, England CG, Nickles RJ, Liu Z, Wang T, Cai W, Nanoscale, 2016; 8: 12683.

[159]. Liu T, Shi S, Liang C, Shen S, Cheng L, Wang C, Song X, Goel S, Barnhart TE, Cai W, ACS Nano, 2015; 9: 950

[160]. Lin J, Wang M, Hu H, Yang X, Wen B, Wang Z, Jacobson O, Song J, Zhang G, Niu G, Huang P, Chen X, Adv Mater, 2016; 28: 3273.

[161]. Hergt R, Dutz J, Magn Magn Mater, 2007; 311: 187.

[162]. Guardia P, Di Corato R, Lartigue, Wilhelm L, Espinosa C, Garcia-Hernandez A, Gazeau M, Manna F, Pellegrino L, ACS Nano, 2012; 6: 3080.

[163]. Salunkhe B, Khot M, Pawar H, Curr Top Med Chem, 2014; 14: 572.

[164]. Jian L, Shi Y, Liang J, Liu C, Xu G, IEEE Trans Appl Supercond, 2013; 23: 4400104.

[165]. Tasci TO, Vargel I, Arat A, Guzel E, Korkusuz P, Atalar E. Med Phys, 2009; 36: 1906.

[166]. Garcia-Jimeno S, Ortega-Palacios R, Cepeda-Rubio MFJ, Vera A, Leija L, Estelrich J, Prog Electromagn. Res, 2012; 128: 229.

[167]. Jordan A, Scholz R., Wust P, Fahling H, Felix R, J Magn Magn Mater, 1999; 201: 413.

[168]. Huang H, Delikanli S, Zeng H, Ferkey DM, Pralle A, Nat Nanotechnol 2010; 5: 602.

[169]. Polo-Corrales L, Rinaldi C J, Appl Phys, 2012; 111: 07B334.

[170]. Dias JT, Moros M., del Pino P, Rivera S, Grazu V, de la Fuente J M, Angew Chem Int. Ed, 2013; 52: 11526.

[171]. Riedinger A, Guardia P, Curcio A, Garcia MA, Cingolani R, Manna L, Pellegrino T, Nano Lett, 2013; 13: 2399.

[172]. Brites CDS, Lima PP, Silva NJO, Millan A, Amaral VS, Palacio F, Carlos LD, Adv Mater, 2010; 22: 4499.

[173]. Sharma R., Chen CJ, Nanopart Res, 2009; 11: 671.

[174]. Hilger I, Hiergeist R, Hergt R, Winnefeld K, Schubert H, Kaiser WA, Invest Radiol, 2002; 37: 580.

[175]. Lee JH, Jang JT, Choi JS, Moon SH, Noh SH, Kim JW, Kim JG, Kim IS, Park KI, Cheon J, Nat Nanotechnol, 2011; 6: 418.

[176]. Van der Zee J, Ann Oncol, 2002; 13: 1173.

[177]. Fajardo F, Cancer Res, 1984; 44:4826s.

[178]. Deatsch E, Evans AJ, Magn Magn Mater, 2014; 354: 163.

[179]. O'Neill KL, Fairbairn DW, Smith MJ, Poe BS, Apoptosis, 1998; 3: 369.

[180]. Harmon BV, Corder AM, Collins RJ, Gobe GC, Allen J, Allan D, Kerr JFR., Int J Radiat Biol, 1990; 58: 845.

[181]. Kanduc D, Mittelman A, Serpico R, Sinigaglia E, Sinha A, Natale C, Santacroce R, Di Corcia M, Lucchese A, Dini L, Pani P, Santacroce S, Simone S, Bucci R, Farber E, Int J Oncol, 2002; 21: 165.

[182]. Farber E, Mod Pathol, 1994; 7: 605.

[183]. Thiesen B, Int J Hyperthermia, 2008; 24: 467.

[184]. Giri J, Ray A, Dasgupta S, Datta D, Bahadur D, Bio-Med Mater Eng, 2003; 13: 387.

[185]. Kuznetsov AA, Leontiev VG, Brukvin VA, Vorozhtsov GN, Kogan BY, Shlyakhtin OA, Yunin AM, Tsybin OI.; Kuznetsov OA, J Magn Magn Mater, 2007; 311: 197

[186]. Shimizu T, Asano H, Matsui MJ, Magn Magn Mater 2007; 310: 1835.

[187]. Shlyakhtin OA, Leontiev VG, Oh YJ, Kuznetsov A, Smart Mater Struct, 2007; 16: N35.

[188]. Prasad NK, Rathinasamy K, Panda D, Bahadur DJ, Biomed Mater Res Part B, 2008; 85: 409.

[189]. Saito H, Mitobe K. Ito A, Sugawara Y, Maruyama K, Minamiya Y, Motoyama S, Yoshimura, N, Ogawa I, Cancer Sci. 2008; 99: 805.

[190]. Apostolov A, Apostolova I, Wesselinowa J,·J Appl Phys 2011; 109: 083939.

[191]. Creixell M, Bohorquez A, Torres-Lugo M, Rinaldi C, ACS Nano 2011; 5: 7124.

[192]. Hayashi K, Nakamura M, Sakamoto W, Yogo T, Miki H, Ozaki S, Abe M, Matsumoto T, Ishimura K, Theranostics, 2013; 3: 366.

[193]. DeNardo SJ, DeNardo GL, Miers LA, Natarajan A, Foreman AR, Gruettner C, Adamson GN, Ivkov R, Clin Cancer Res, 2005; 11: 7087s.

[194]. Yin PT, Shah BP, Lee KB, Small, 2014, 10: 4106.

[195]. Cervadoro A, Cho M, Key J, Cooper C, Stigliano C, Aryal S, Brazdeikis A, Leary JF, Decuzzi P, ACS Appl Mater Interfaces, 2014 , 6: 12939.

[196]. Fantechi E, Innocenti C, Zanardelli M, Fittipaldi M, Falvo E, Carbo M, Shullani V, Di Cesare M, Ghelardini L, Ferretti C, Ponti A, Sangregorio C, Ceci P, ACS Nano, 2014; 8:4705.

[197]. Maity D, Chandrasekharan P, Pradhan P, Chuang KH, Xue JM, Feng, SS, Ding J, J Mater Chem, 2011; 21: 14680

[198]. Majeed J, Pradhan L, Ningthoujam S, Vatsa K, Bahadur D, Tyagi K, Colloids Surf B: Biointerfaces, 2014; 122: 396.

[199]. Gkanas I, Cent Eur J Chem, 2013; 11: 1042.

[200]. Jadhav V, Prasad I, Kumar A, Mishra R, Dhara S, Babu R, Prajapat L, Misra L, Ningthoujam S, Pandey N, Vatsa K, Colloids Surf B: Biointerfaces, 2013;108: 158.

[201]. Khandhar P, Ferguson M, Simon A, Krishnan M, J. Appl. Phys, 2012; 111: 07B306.

[202]. Swain .K, Pradhan L, Bahadur, D, ACS Appl Mater Interfaces, 2015; 7: 8013.

[203]. Basel T, Balivada S, Wang H, Shrestha B, Seo M, Pyle M, Abayaweera G, Dani R, Koper B, Tamura M, Chikan V, Bossmann H, Troyer L,Int J Nanomed, 2012; 7; 297

[204]. Huang S, Hainfeld F, Int J Nanomed, 2013; 8: 2521

[205]. Hayashi K, Nakamura M, Miki H, Ozaki S, Abe M, Matsumoto T, Sakamoto W, Yogo T, Ishimura K,Theranostics, 2014; 4: 834.

[206]. Ling Y, Tang X, Wang F, Zhou X, Wang R, Deng L Shang T, Liang B, Li P, Ran H, Wang Z,Hu B, Li C, Zuo G, Zheng Y, RSC Adv, 2017; 7: 2913.

[207]. Grillo R, Gallo J, Stroppa D, Carbó-Argibay E, Lima R, Fraceto L, Bañobre-López M, ACS Appl Mater Interfaces, 2016; 8: 25777.

[208]. Cristofolini L, Szczepanowicz K, Orsi D, Rimoldi T, Albertini F, Warszynski P, ACS Appl Mater Interfaces, 2016; 8: 25043.

[209]. Lattuada M, Hatton TA, Langmuir, 2007; 23: 2158.

[210]. Monnier C, Burnand D, Rothen-Rutishauser D, Lattuada M, Petri-Fink A, Eur J Nanomed, 2014; 6: 201.

[211]. Di Corato R, Béalle G, Kolosnjaj-Tabi J, Espinosa A, Clément O, Silva A, Ménager C,Wilhelm C, ACS Nano, 2015; 9: 2904.

[212]. Kandasami G, Maity D, Int J Pharmaceut, 2015; 496: 191.

[213]. Huang C, Liao Z, Lu H, Pan W, Wan W, Chen C, Sung H, Chem Mater, 2016; 28: 9017.

[214]. Lee H, Lee E, Kim K, Jang N, Jeong Y,Jon S, J Am Chem Soc, 2006; 128: 7383.

[215]. Cheng Y, Su H, Yang S, Yeh S, Tsai Y, Wu L, Wu T, Shieh B, Biomaterials, 2005; 26: 729.

[216]. Khan I, Mohammad A, Patil G, Naqvi H, Chauhan S, Ahmad I, Biomaterials, 2012; 33: 1477.

[217]. Wydra, R. J.; Rychahou G, Evers M; Anderson W, Dziubla D, Hilt Z, Acta Biomater, 2015; 25: 284.

[218]. Clift J, Gehr P, Rothen-Rutishauser B, Arch Toxicol, 2011; 85: 723.

[219]. Smith T, Environ. Health Perspect, 1996; 104: 1219.

[220]. Mahmoudi M, Hofmann H, Rothen-Rutishauser B, Petri-Fink A, Chem Rev, 2012; 112: 2323.

[221]. Weissleder R, Cheng C, Bogdanova A, Bogdanov A, J Magn Reson Imaging, 1997; 7: 258.

[222]. Moore M, Weissleder R, Bogdanov A, J Magn ResonImaging, 1997; 7: 1140.

[223]. Neuwelt A, Weissleder R, Nilaver G, Kroll A, Romangoldstein S, Szumowski J, Pagel A, Jones S, Remsen G, McCormick L, Shannon M, Muldoon, Neurosurgery,1996; 34: 777.

[224]. Mueller H, Maassen S, Weyhers H,Specht F,Lucks S, Int J Pharm, 1996; 138: 85.

[225]. Berry C, Wells S, Charles S, Aitchison G, Curtis G, Biomaterials, 2004; 25: 5405.

[226]. Gupta K, Berry C, Gupta M, Curtis A, IEEE Trans.Nanobiosci. 2003; 2: 255.

[227]. Gupta K, Curtis G, Biomaterials, 2004; 25: 3029.

[228]. Gupta K, Naregalkar R., Vaidya D, Gupta M, Nanomedicine, 2007; 2: 23.

[229]. van den Bos J, Wagner A, Mahrholdt H, Thompson B, Morimoto Y, Sutton S, Judd M, Taylor A, Cell Transplant, 2003; 12: 743.

[230]. Stroh A, Zimmer C, Gutzeit C, Jakstadt M, Marschinke F, Jung T, Pilgrimm H, Grune, T, Free Radical Biol Med, 2004; 36: 976.

[231]. Brunner J, Wick P, Manser P,Spohn P, Grass N, Limbach K, Bruinink A, Stark W, J Environ Sci Technol, 2006;40: 4374.

[232]. Soto K, Carrasco A., Powell G, Garza M, Murr E, J. Nanopart. Res. 2005; 7: 145.

[233]. Soto F, Garza M., Murr E, Acta Biomater. 2007; 3: 351.

[234]. Jeng A, Swanson J, J Environ Sci Health, 2006; 41: 2699.

[235]. Au C, Mutkus L,Dobson A, Riffle J, Lall J, Aschner M, Biol Trace Elem Res, 2007; 12: 248.

[236]. Pisanic R, Blackwell D, Shubayev I, Finones R, Jin, S, Biomaterials, 2007; 28: 2572.

[237]. Raynal, Prigent I, Peyramaure P, Najid S , Rebuzzi A, Corot C, Invest Radiol, 2004; 39: 56.

[238]. Diaz B, Sanchez-Espinel C, Arrueho M, Faro J, DeMiguel E, Magadan S, Yague C, Fernandez-Pachecco R, Ibarr R, Santamaria J, Gonzales-Fernandez A, Small, 2008; 4: 2025.

[239]. de la Fuente M, Alcantara D, Penades S, IEEE Trans.Nanobiosci, 2007; 6: 275.

[240]. Alekseenko V, Wassem V, Fedorovich V, Brain Res, 2008; 1241: 193.

[241]. Theil C, Matzapetakis M., Liu F, J Biol Inorg Chem, 2006; 11: 803.

[242]. Li N, Sioutas C, Cho A, Schmitz D, Misra C, Sempf J, Wang M, Oberley T, Froines J, Nel A, Environ. Health Perspect., 2003;111: 455.

[243]. Amara N, Bachoual R, Desmard M, Golda S, Guichard C, Lanone S, Aubier M, Ogier-Denis M, Boczkowski E, Lung Cell Mol. Physiol, 2007; 293: L170.

[244]. Arimoto T, Kadiiska B, Sato K, Corbett J., Mason , P.Am. J. Respir. Crit. Care Med. 2005; 171:379.

[245]. Ruehm, S. G.; Corot, C.; Vogt, P.; Kolb, S.; Debatin JF, Circulation, 2001; 103: 415.

[246]. Zhang Y, Kohler N, Zhang Q, Biomaterials, 2002; 23: 1553.

[247]. Kooi E, Cappendijk C, Cleutjens K, Kessels H, Kitslaar P, Borgers M, Frederik M, Daemen M.,van Engelshoven A, Circulation 2003; 107: 2453.

[248]. Siglienti I, Bendszus M, Kleinschmitz C, Stoll C, J Neuroimmunol, 2006; 173: 166.

[249]. Hsiao K, Chu H,Wang H,Lai W, Choii T, Hsieh T, Wang L, Liu M, NMR Biomed, 2008; 21: 820.

[250]. Naveau A, Smirnov P, Menager C, Gazeau F, Clement O, Lafont A, Gogly B, J. Periodontol. 2006; 77:238.

[251]. Radu M, Munteanu MC, Petrache S, Serban AI, Dinu D, Hermenean A, Sima C, Dinischiotu A, Acta Biochim Pol. 2010; 57: 355.

[252]. Choi Y, Lee H, Na,B, An K., Hyeon T, Seo S,Bioprocess Biosyst Eng, 2010; 33: 21.

[253]. Natarajan A, Gruettner C, Ivkov R., Denardo L, Mirick G, Yuan A, Foreman A, De NardoS, J Bioconjugate Chem, 2008;19: 1211.

[254]. Jain K, Reddy K, Morales A, Leslie-Pelecky L, Labhasetwar V, Mol Pharmaceutics, 2008; 5: 316.

[255]. Weissleder R, Stark D, Engelstad L, Bacon R, Compton C, White L, Jacobs P, Lewis J, Am . Roentgenol,1989; 152: 167.

[256]. Mahmoudi M, Laurent S, Shokrgozar A, Hosseinkhani M, ACS Nano 2011; 5: 7263.

[257]. Hanini, A, Schmitt, A, Kacem K, Chau F, Ammar S, Gavard J. Int. J. Nanomed., 2011, 6: 787.

[258]. Chertok B, Moffat A, David E, Yu F, Bergemann C, Ross D, Yang C, Biomaterials, 2008, 29: 487.

[259]. Faraudo J, Andreu J S, Calero C, Camacho J, Adv Funct Mater, 2016, 26: 3837.

[260]. Allen MP, Tildesley DJ: Computer simulation of liquids. Oxford; 1989.

[261]. Frenkel D, Smit B, Understanding molecular simulation: from algorithms to applications. 2nd ed. San Diego: Academic Press; 2002.

[262]. Metropolis N, Rosenbluth A W, Marshall N, Rosenbluth MN, Teller AT, J Chem Phys, 1953, 21:1087.

[263]. Qiang L, Li Z, Zhao T, Zhong S, Wang H, Cui X, Colloids and Surfaces A: Physicochem Eng Aspects, 2013; 419: 125.

[264]. Qiang L, Yang T, Li Z, Wang H, Chen X, Cui X, Colloids and Surfaces A: Physicochemical and Engineering Aspects, 2014, 456: 62.

[265]. Harris R A, van der Walt H, Shumbula P M, J Mol Str, 2013; 1048: 18.

[266]. Harris R A, Shumbula P M, van der Walt H, Langmuir, 2015; 31: 3934.

[267]. Yue J, Jiang X, Yu A, J Phys Chem B, 2011; 115: 11693.

[268]. Yu S, Perálvarez-Marín A, Minelli C, Faraudo J, Roig A, Laromaine A, Nanoscale, 2016, 8: 14393.

[269]. Pedram MZ, Shamloo A, Alasty A, Ghafar-Zadeh E, Biosensors, 2016; 6: 25.

[270]. Tombácz E, Hajdú A, Illés E, Langmuir, 2009; 25: 13007.

[271]. Kumar S, Ravikumar C, Bandyopadhyaya R, Langmuir, 2010; 26: 18320.

[272]. Matsumoto Y, Jasanoff A, Magnetic Resonance Imaging, 2008; 26: 994.

[273]. Martinez-Boubeta C, Simeonidis K, Makridis A, Angelakeris M, Iglesias O, Guardia P, Cabot A, Yedra L, Estrade S, Peiro F, Saghi Z, Midgley P A, Conde-Leborán I, Serantes D, Baldomir D, Sci Reports, 2013; 3: 1652.

[274]. Russier V, de Montferrand C, Lalatonne Y, Motte L, J Appl Phys, 2012; 112: 073926.

[275]. Castro LL, Gonçalves GRR, Skeff Neto K, Morais PC, Bakuzis AF, Miotto R, Phys Rev E, 2008; 78: 061507.

[276]. Aschauer U, Selloni A, J Chem Phys, 2015 ; 143: 044705.

[277]. Guénin E, Lalatonne Y, Bolley J, Milosevic I, Platas-Iglesias C, Motte L, J Nanopart Res, 2014; 16: 2596.

[278]. Fouineau J, Brymora K, Ourry L, Mammeri F, Yaacoub N, Calvayrac F, Ammar S, Greneche JM, J Phys Chem C, 2013; 117: 14295.

[279]. de Leeuw N, Cooper T , Geochim Cosmochim Ac, 2007; 71: 1655.

[280]. Andreu JS, Camacho J, Faraudo J, Benelmekki M, Rebollo C, Martínez LM, Phys Rev E, 2011; 84: 021402.

[281]. Faraudo J, Camacho J, Colloid Polym Sci, 2010; 288: 207.

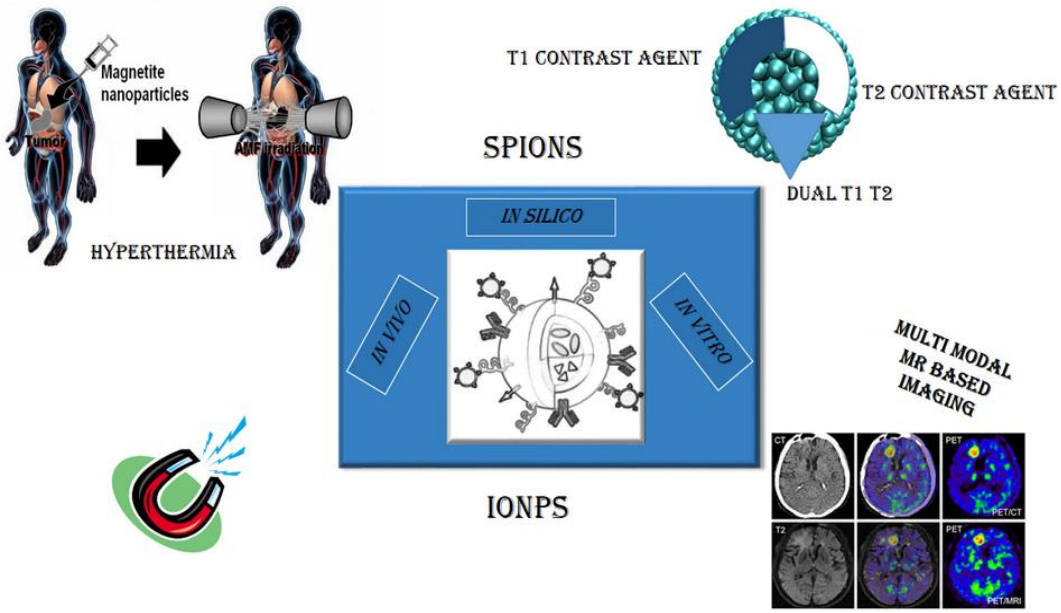

Graphical Abstract

Highlights

- ✓ Review of current computational methods for IONPs
- ✓ IONPs as a MRI and multimodal imaging platform
- ✓ Magnetoresponsive therapy – hyperthermia
- ✓ Toxicological evaluation of IONPs in *in vivo* and *in vitro* studies